2017

KNOCKOUT OF SPHINGOSINE KINASE 1 ATTENUATES RENAL INTERSTITIAL FIBROSIS IN UNILATERAL URETERAL OBSTRUCTION (UUO) MODEL

Xiwen Zhang
Virginia Commonwealth University

KNOCKOUT OF SPHINGOSINE KINASE 1 ATTENUATES RENAL INTERSTITIAL FIBROSIS IN UNILATERAL URETERAL OBSTRUCTION (UUO) MODEL

A thesis submitted in partial fulfillment of the requirements for the degree of Master of Science at Virginia Commonwealth University

By

Xiwen Zhang

Bachelor of Science in pharmaceutics

Shenyang Pharmaceutical University, 2015

Director: Ningjun Li, MD

Associate professor, Pharmacology and Toxicology

Virginia Commonwealth University

Richmond, Virginia

July, 2017

ACKNOWLEDGEMENT

There are no words to fully express the deep gratitude I feel towards everyone who has supported me throughout this incredible journey. Attaining this degree is the product of the hard work of many, and I have been extremely fortunate to come across so many people willing to help me achieve this milestone. First and foremost, my sincerest thanks to Dr. Ningjun Li for going above and beyond what is expected of a mentor and providing me a wonder place to do research. My training and this study could not have been made possible without the help from many past and present members of the lab, especially Dr. Fan Wang, Weili Wang and Dr. Junping Hu for their early guidance when I got in lab at first beginning and Guangbi Li, Ashley Pitzer, and Dr. Sabena Conley for helping me settle down in our department. Thanks to Dr. Pin-Lan Li's support, as her lab staff and equipment helped much. In addition, thanks to Dr. Xinxu Yuan, Dr. Nan Meng, Dr. Qinghua Zhang, Dr. Rami Lee and Dr. Owais Bhat for sharing with me their expertise and being prime examples of honest and hardworking scientists. My sincere thanks to my committee members, Dr. Joseph Ritter and Dr. Siddhartha Ghosh, who I have gotten the pleasure of knowing over the past two years. Their insightful expertise, constructive criticism, and advice on my research proposal have been invaluable throughout the course of these studies and in the preparation of this dissertation.

TABLE OF CONTENT

LIST OF FIGURES

LIST OF ABBREVIATIONS

S1P	sphingosine-1-phosphate
UUO	unilateral ureteral obstruction
SphK1	sphingosine kinase 1
ER	endoplasmic reticulum
ERK	extracellular signal-regulated kinase
PLC	phospholipase C
PI3K	phosphatidylinositol 3-kinase
TGF-β	transforming growth factor-β
α-SMA	α-smooth muscle actin
S1PRs	S1P receptors
ECM	extracellular matrix
EMT	epithelial-to-mesenchymal transition
EndoMT	endothelial-to-mesenchymal transition
CTGF	connective tissue growth factor
GFR	glomerular filtration rate
PDGF	platelet-derived growth factor
CKD	chronic kidney disease
KO	knockout
PAS staining	Periodic-Acid Schiff staining
NF-κB	nuclear factor kappa-light-chain-enhancer of activated B cells
STAT3	signal transducer and activator of transcription 3

HIF-1α   hypoxia-inducible factor-1α

PHD2   proly hydroxylase domain-containing protein 2

ABSTRACT

KNOCKOUT OF SPHINGOSINE KINASE 1 ATTENUATES RENAL INTERSTITIAL

FIBROSIS IN UNILATERAL URETERAL OBSTRUCTION (UUO) MODEL

By Xiwen Zhang, B.S.

A thesis submitted in partial fulfillment of the requirements for the degree of Master of

Science at Virginia Commonwealth University

Virginia Commonwealth University, 2017

Major Director: Ningjun Li, MD, Associate Professor, Pharmacology and Toxicology

Sphingosine-1-phosphate (S1P) is a bioactive sphingolipid metabolite and an important

signaling molecule that plays a significant role in the differentiation of fibroblasts to

myofibroblasts, which is seen as a crucial process during fibrogenesis. S1P synthesis is

catalyzed by sphingosine kinases (SphKs), which phosphorylate sphingosine into S1P.

The present study tested the hypothesis that SphK1-S1P signaling pathway participates in the kidney damage in unilateral ureteral obstruction (UUO) model using SphK1 knockout mice. UUO was created by ligation of the ureter on one kidney and the unobstructed contralateral kidney is used as control. Wild type C57BL6 mice and SphK1 KO mice were subjected to UUO for 7 days or 14 days and then four groups of kidneys were collected: wild type control group (WT-C), wild type UUO group (WT-UUO), SphK1$^{-/-}$ control group (KO-C) and SphK1$^{-/-}$ UUO group (KO-UUO). The mRNA level of SphK1 in WT-UUO was increased by 6.1 folds compared to control groups and there was no significant difference between the other three groups. The markers of fibrosis, α-smooth muscle actin (α-SMA) and collagen I, were both upregulated in UUO groups, whereas the levels of these two proteins were significant lower in KO-UUO than that WT-UUO. The immunohistochemistry analyses showed that the positive staining of α-SMA and collagen was located in the interstitial space and the infiltration of immune cells normalized with the WT-C, CD43- and CD68- positive cells were higher in UUO groups than in control groups, but there was no significant difference between KO-UUO and WT-UUO. This suggests that the differences of renal fibrotic markers between WT-UUO and KO-UUO are not due to the change of immune regulation by knockout of SphK1, rather, it is the direct effect of the deficiency of SphK1 on kidney tissue. Further, the morphological examination showed that the tubular injury score and glomerular damage index were much higher in UUO groups, but the kidney damage indices were significantly decreased in KO-UUO compared with WT-UUO. These results suggest that SphK1-S1P signaling pathway mediates kidney damage in UUO mice. Manipulating SphK1-S1P signaling pathway may be used as a therapeutic strategy in renal interstitial fibrosis.

CHAPTER ONE

INTRODUCTION

1.1 Introduction of S1P

Sphingolipids, compounds that contain a long-chain sphingoid base [1], have gained considerable attention during the last decades since they not only serve as structural components of cell membrane but also elicit important functions as signaling molecules, which regulate biological functions in both intracellular and extracellular compartments. The kidney is an important tissue serving for sphingolipids studies because of the unique wide expression of glycosphingolipids. Glycophingolipids are ceramides with one or more sugar residues joined in a β-glycosidic linkage at the 1-hydroxyl position [2]. S1P is produced by sphingosine kinases that phosphorylate sphingosine and is now recognized as a critical regulator of physiological and pathophysiological processes, including atherosclerosis, respiratory distress, diabetes, cancer and inflammatory disorders [3-6]. It also participates in diverse cellular behaviors such as cell adhesion, migration, proliferation and differentiation. S1P targets five G-protein-coupled receptors named S1PR1-5, which are distributed in different tissues and organs. In addition, coexpression of S1P receptors and promiscuous coupling generates variable and complex signals [7].

1.1.1 Metabolism of Sphingolipids

Sphingosine-1-phosphate (S1P) was originally considered as an intermediate product during the detoxification of sphingosine. S1P synthesis is catalyzed by sphingosine kinases. Nowadays, two isozymes of sphingosine kinases, known as SphK1 and SphK2 [8] have been identified, which catalyze the phosphorylation of D-erythro-sphingosine and produce S1P, using ATP as phosphate donor. S1P can be converted back to sphingosine by S1P phosphatases (SPP1 and SPP2) [9] located in the endoplasmic reticulum (ER) or lipid phosphate phosphatases (LPP1-LPP3) existing on the plasma membrane [10]. S1P is further degraded by S1P lyase (SPL) into ethanolamine phosphate and hexadecenal [11], which is also located in the ER. The immediate substrate for the generation of S1P, sphingosine, is formed from the hydrolysis of ceramide by ceramidase and most of sphingosine is synthesized from this salvaged pathway by the deacylation of ceramide [12, 13]. Ceramide is the central building block of all sphingolipids and its *de novo* synthesis is from the condensation of amino acid L-serine and

Figure 1. Biosynthesis of S1P pathway

palmitoyl-CoA in the ER. In the catabolic pathway, ceramide is released from hydrolysis of sphingomyelin by sphingomyelinases that is located in the cell membrane [14], which is a more rapid way to generate ceramide than *de novo* synthesis pathway. Meanwhile,

ceramide can be converted back to sphingomyelin via transferring phosphocholine from phosphatidylcholine to ceramide, which is catalyzed by sphingomyelin synthase [1]. **Figure 1** shows the general pathway of sphingolipids syntheses and metabolites [15]. The conversion among ceramide, sphingosine and S1P serves as 'sphingolipid rheostat' and the modulation of this 'sphingolipid rheostat' plays roles in cell fate determination as well as the progression and drug sensitivity of cancer, and may act as treatment strategies against cancer [16]. There is a concentration gradient among these three metabolites, with ceramide presenting the highest and S1P the lowest level. A small change in ceramide concentration significantly affects the concentration of sphingosine and S1P. Therefore, the generation of S1P is not only regulated by biosynthetic and degradative enzymes but also by availability of the upstream substrates.

1.1.2 Intracellular and extracellular S1P

S1P is synthesized intracellularly and then acts as a bioactive molecule in intracellular or extracellular pathways. As an extracellular bioactive molecule, cytosolic S1P synthesis is catalyzed by SphK1 [17]. Once S1P is formed in cytosol, it will be exported out of the cell by several transporters including the ATP-binding cassette transporters: ABCA, ABCC1, ABCG2 [18, 19], and the putative transporter Spinster 2 [20]. The extracellular S1P targets its receptors on the plasma membrane to mediate extracellular signaling pathways. Most of S1P in circulatory system of body is bound to acceptor plasma proteins. The majority of these plasma proteins are high-density lipoprotein (HDL) and albumin [21-23]. The effects of S1P are mostly mediated by its cell surface receptors.

However, there is evidence, though limited, showing that S1P may also act as an intracellular messenger. It has been demonstrated that S1P produced by SphK2 on the ER membrane [24] mediates intracellular pathway, which plays a crucial role in counteracting apoptosis. In addition to apoptosis [25], S1P as a second messenger in the cell also activates calcium channels, regulates inflammatory responses, promotes cell survival, and reduces tumor progression and size etc., though no direct intracellular target for S1P has been found [26].

1.1.3 S1P receptors

To date, there are five specific subtypes of S1P G-protein-coupled receptors identified: S1PR1/EDG1, S1PR2/EDG5, S1PR3/EDG3, S1PR4/EDG6, and S1PR5/EDG8, which are coupled with various G-proteins. These G-proteins regulate different downstream molecules of signaling pathways, such as adenylyl cyclase (AC), cyclic AMP (cAMP), extracellular signal-regulated kinase (ERK), phospholipase C (PLC), phosphatidylinositol 3-kinase (PI3K), the small GTPases of the Rho family and Jun amino terminal kinase (JNK) etc. [27, 28]. Like other G-protein-coupled receptors, S1P receptors are composed of seven-transmembrane helices arranged in a structurally conserved bundle with three loops located in extracellular domains [29]. However, these five subtypes of S1P receptors have different patterns of expression in various tissues. For example, S1PR1-S1PR3 are expressed in almost all the tissues, but S1PR4 and S1PR5 are expressed in lymphoid and in brain respectively [30].

Coupling S1PR1 with heterotrimeric G_i activates PI3-kinase-Akt/Rac pathway, which initiates cell migration. S1PR1 coupled with G_i also activates Ras-ERK pathway, which

stimulates cell proliferation and moderately activates phospholipase C that initiates Ca^{2+} mobilization [31, 32]. In contrast, S1PR2 is coupled with G_i, $G_{12/13}$, and G_q. S1PR2 coupled with $G_{12/13}$ activates Rho leading to the inhibition of Rac pathway and cell migration. S1PR2 coupled with G_{13} also stimulates adenylate cyclase. In addition to being coupled with $G_{12/13}$, S1PR2 activates G_q-PLC-Ca^{2+} and G_i-Ras-ERK pathways to initiate release of Ca^{2+} [33] from intracellular stores to stimulate cell proliferation. S1PR3 also activates G_i-PI3-kinase-Akt/Rac pathways to stimulate cell migration [34, 35].

S1PR4 is primarily expressed in lymphoid tissue, which is coupled with G_i to mediate activation of ERK and PLC stimulation and with $G_{12/13}$ to activate Rho pathway. The previous study stated that in S1PR4 KO mice, the deficiency of S1PR4 has profound effect on dendritic cell migration, cytokine secretion and inhibits differentiation of T helper cells (Th cells) [36]. S1PR5 is mainly expressed in brain and highly expressed in blood−brain barrier endothelial cells to maintain the integrity of barrier, which can serve as a novel strategy for treatment of Alzheimer's or multiple sclerosis [37]. S1PR5 is also expressed in oligodendrocytes and oligodendrocyte precursor cells (OPCs). The activation of S1PR5 causes migration of oligodendrocyte progenitor to be inhibited [38]. Based on the interaction of potential functions of S1P receptors, these downstream signaling pathways provide multiple alternatives to control various diseases.

1.1.4 S1P in kidney diseases

It has been shown that there is a rank order in the expression of S1P receptors in whole mouse kidney tissue: S1PR1>S1PR3>S1PR2>S1PR4 with no S1PR5 mRNA expression [39]. Nowadays, a large number of studies have shown that S1P regulates multiple kidney

injuries and diseases, such as ischemia-reperfusion injury, diabetic nephropathy, glomerulonephritis, nephroblastoma and renal fibrosis by participating in cellular signaling pathways in different cell types. Diabetic nephropathy causes a local S1P increase in rat kidney. Furthermore, some researchers have demonstrated that activation of S1PR1 protects kidney injuries from early stage of diabetic nephropathy. In addition, activation of S1PR1 protects kidney from renal-ischemia-reperfusion injury by inhibiting infiltration of T-cells [39-42]. However, inhibition of S1PR2 attenuates renal injury from ischemia-reperfusion injury [43]. Interestingly, S1P can also induce kidney injury by targeting S1PR2. This increases the expression of cyclooxygenase-2 (COX-2) and prostaglandin E2 (PGE$_2$) to upregulate kidney mesangial cells migration, which is associated with glomerular injury [44, 45]. In addition, a previous study has shown that S1P in kidney mesangial cells is associated with progression of fibrogenesis by activating S1PR2 or S1PR3 to mimic transforming growth factor beta (TGF-β)/Smad pathway [46, 47]. Our study was focused on whether SphK1/S1P mediates renal interstitial fibrosis.

1.2 General introduction of fibrosis

Generally, the consequences of chronic kidney disease (CKD) are glomerulosclerosis and tubulointerstitial fibrosis. The glomerulosclerosis, despite being a disease with its own entity, causes tubulointerstitial fibrosis by inducing tubular destruction. Thus, renal fibrosis can also be considered as tubulointerstitial fibrosis since this process features tubular destruction [48]. Tubulointerstitial fibrosis is normally generated by chronic inflammatory response. Early stage of fibrogenesis is seen as dysfunction of wound healing. The stages of wound healing produce provisional extracellular matrix (ECM) to coordinate the four phases of wound healing: hemostasis, inflammation, proliferation, and remodeling

6

after the damage of endothelial cells or epithelial cells [49]. With duration of injury, ECM is remodeled and difficult to degrade, which contributes to forming fibrous tissue and becoming irreversible fibrosis [50]. Renal interstitial fibrosis can be separated into 4 stages: priming, activation, execution and progression. Yet, there is no clear boundary among these 4 stages and each stage has their specific molecular and cellular mechanisms [51].

In Chronic kidney disease, the immune cells infiltrate into injury tissues such as macrophage-innate immune cells and T cells-adaptive immune cells, which to destroys and removes pathogens and initiate the other four following stages. Priming is the early stage of fibrotic diseases with infiltration of lymphocytes, monocytes, macrophages, dendritic cells and mast cells into kidney. Under unresolving situations, immune cells are triggered to secrete cytokines and further induce kidney fibrogenesis and kidney injury [52, 53]. Activation is a process that converts normal cells to acquire myofibroblast phenotypes. Myofibroblasts produce a large amount of extracellular matrix into interstitial space that are considered to be the primary source of ECM deposition and play a crucial role in wound healing and remodeling tissue with α-SMA being expressed in myofibroblasts [54]. Execution is involved in ECM protein synthesis, secretion, invasion in the interstitial space. During this stage, ECM starts to resist degradation after being modified. Execution is recognized as an early stage of the fibrosis, which can theoretically be treated to reverse fibrosis [55]. Progression is the stage for development of fibrogenesis. This stage involves multiple cellular and molecular mechanisms, which

7

contributes to the excessive ECM production and tubular injury and atrophy, microvascular rarefaction, chronic hypoxia etc. [56, 57].

However, it should be noted that the origins of myofibroblasts remain debated. It has been shown that there are at least five sources of myofibroblasts such as activation from interstitial fibroblasts, differentiation from pericytes, recruitment of fibrocytes and the other mechanisms collectively called epithelial-to-mesenchymal transition (EMT) and endothelial-to-mesenchymal transition (EndoMT) [58]. It is difficult to track how different types of cells become myofibroblasts due to lack of cell markers. In conclusion, how phenotypes of cells are changed into myofibroblasts and the main sources of myofibroblasts are still a controversial topic.

At present, strong evidence suggests that TGF-β/Smad signaling is a key pathway in renal fibrosis and participates in the stage of activation and execution because it not only regulates the production and degradation of ECM but also mediates EMT process [59]. TGF-β is synthesized from inflammatory cells that infiltrate injured tissue. The secreted TGF-β binds to its receptors that are located on cell membrane in different cell types and then the downstream molecules Smad2, Smad3 are phosphorylated and activated to interact with Smad4 forming a complex. The Smad complex will be translocated into nucleus and regulate the transcription of its target genes such as connective tissue growth factor (CTGF), fibronectin, type I collagen, vimentin, α-SMA. During this process, the phenotypic characterizations of the cell are changed into myofibroblasts with vimentin and α-SMA being expressed in the cells and losing cell-cell adhesion. As a result, the cells

acquire the ability to migrate and proliferate, which is termed cell dedifferentiation [60, 61]. Myofibroblasts produce extracellular matrix protein such as collagen I and fibronectin. CTGF is also produced by myofibroblasts to further amplify fibrogenesis [62].

1.2.1 Chronic kidney disease and renal interstitial fibrosis

Chronic kidney disease (CKD) as common conditions of cardiovascular diseases has high prevalence in America, which is mainly correlated with obesity, old age, diabetes, hypertension and other cardiovascular diseases [63]. Glomerular filtration rate (GFR) is used to indicate renal function and is approximately measured by creatinine clearance. In healthy individuals, the GFR ranges from 90 to 120 mL/min/1.73 m^2 in women and 100 to 130 mL/min/1.73 m^2 in men. CKD is defined as GFR below 60 mL/min/1.73 m^2 along with urine albumin–creatinine ratio of at least 30 mg/g. There are five stages of CKD. Stage 1 is defined as GFR above 90 mL/min/1.73 m^2. Stage 2 is GFR ranging from 60 to 89 mL/min/1.73 m^2. Stage 1 and stage 2 usually have no symptoms to indicate the kidney damage. Symptoms of CKD start from Stage 3. Stages 3, 4, and 5 are GFR of 30 to 59 mL/min/1.73 m^2, 15 to 29 mL/min/1.73 m^2, and less than 15 mL/min/1.73 m^2, respectively [64]. Stage 5 is seen as end-stage renal disease (ESRD), which is the kidney failure stage and requires treatment through dialysis or transplantation [65, 66].

Renal fibrosis, particularly interstitial fibrosis with excessive extracellular matrix (ECM) deposition in tubulointerstitial space, is recognized as the end-stage in multiple chronic kidney diseases. The common causes of CKD are obesity, hypertension and diabetes. Obesity can directly induce CKD or indirectly through outcomes that cause diabetes and hypertension [67]. Since obesity is usually followed with diabetes, hypertension or other

cardiovascular diseases, these diseases contribute to CKD directly, while the mechanisms of obesity inducing CKD are unclear. Recently, studies have shown that obesity can be used as an independent risk factor of CKD through inflammation, lipotoxicity, hemodynamic effects or other unknown mechanisms to induce CKD. Diabetes and hypertension are independent factors to induce CKD. These lead to glomerular expansion and cause endothelial dysfunction and hemodynamic changes through: loss of the glomerular basement membrane electric charge and its thickening, a decreased number of podocytes, foot-process effacement and mesangial distension [68]. The progressive renal dysfunction triggers the chronic renal injury that finally induces fibrogenesis.

1.2.2 Renal fibrosis induced by SphK1/ S1P/S1PRs axis

A large amount of accumulating evidence demonstrates that SphK1/S1P/S1PRs axis is a mediator of fibrogenesis such as cardiac fibrosis, pulmonary fibrosis, renal fibrosis, and liver fibrosis [69-71]. The extracellular S1P binds to its receptors S1PRs and induces fibrogenesis by cross communicating with several fibrogenesis pathways. For example, SphK1/S1P/S1PRs axis induces fibrogenesis by interacting with TGF-β/Smad signaling pathway intracellularly. After S1P binds to S1PRs, the Smad is also phosphorylated, which initiates the same downstream TGF-β/Smad signaling to change the phenotypes of cells into myofibroblasts [72]. In addition, it has been found that S1P also interacts with platelet-derived growth factor (PDGF) signaling, which is responsible for proliferation of myofibroblasts and generation of ECM [73, 74]. Besides the direct regulation of fibrosis, SphK1/S1P/S1PRs axis acts as a mediator of pro-inflammatory response in CKD by

promoting the infiltration of inflammatory cells into damaged kidney tissue, which is mediated by the gradients of S1P concentration and S1PRs expression [75].

Although the reports have shown that S1P participates in fibrogenesis in other organs and kidney tissue, there is no direct evidence showing that SphK1/S1P signaling pathway mediates renal fibrosis *in vivo*. Here, the role of SphK1/S1P signaling as a mediator of renal fibrosis was investigated in C57BL/6 mice and SphK1 KO mice using the model of unilateral ureteral obstruction (UUO) in the present study.

1.3 Aims of study

The hypothesis to be tested in the present study states that: knockout of SphK1 prevents kidney damage from UUO due to the inhibition of SphK1/S1P/S1PRs axis signaling with attenuating fibrosis and morphological injury induced by UUO.

The specific aims are:

1. To determine whether SphK1-S1P signaling pathway mediates renal interstitial fibrosis.

2. To determine whether the changes in renal fibrotic markers are due to the immune regulation by knockout of SphK1.

3. To determine whether the morphological injury induced by UUO is attenuated in SphK1 KO mice.

CHAPTER TWO

GENERAL METHODS

2.1 Animals, Unilateral Ureteral Obstruction model, and tissue collection

Experiments were performed in 3 month old 25-30g male C57BL/6 mice and SphK1 KO mice (global knockout) generated on a C57BL/6 background. Mice were purchased from the Jackson Laboratory. Mice were housed in the Animal Care Facility with 12h light/dark cycle in a temperature and humidity controlled facility and had free access to food and water throughout the study. All protocols were approved by the Institutional Animal Care and Use Committee of the Virginia Commonwealth University.

Unilateral Ureteral Obstruction (UUO) surgery was performed as described previously [76]. Mice were anesthetized with inhaled isoflurane (2.5%). The midline longitudinal abdominal incision was performed, which permitted access to the left kidney and ureter. The left ureter was tied twice below the kidney with surgical silk. The mice were sacrificed at either 7 days or 14 days and both sides of kidneys were collected. Special attention was paid to ensure that the point of ligation was identical across animals and that the damage to the kidneys would be the same in UUO kidneys. A diagram of UUO surgical

procedure and Day 14 UUO kidney appearance are shown in **Figure 2** [77]. All the mice underwent UUO surgery in left kidney and that the unobstructed contralateral kidney were used as control. The kidney samples were divided into four groups: Wild type control group (WT-C), wild type UUO group (WT-UUO), SphK1 KO control group (KO-C), SphK1 KO UUO group (KO-UUO). Each group had 5-6 mice.

14 Days
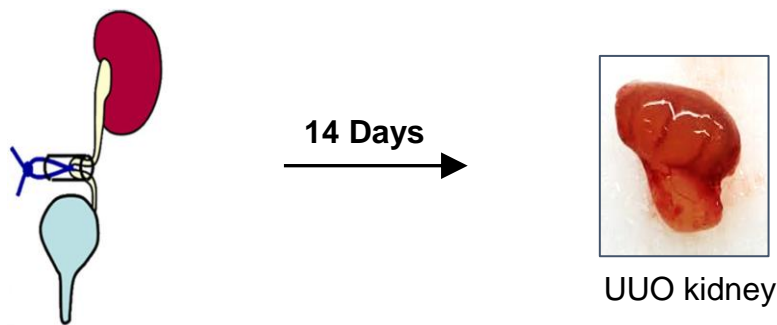
UUO kidney

Figure 2. Diagram of UUO surgical procedure and Day 14 UUO kidney appearance.

2.2 RNA isolation and real time RT-PCR

Total RNA was isolated from mouse kidney tissue using TRIzol reagent (Life Technology, Rockville, MD, USA) according to the manufacturer's instructions. RNA was quantified using Shimadzu UV160U UV-Visible Recording Spectrophotometer by 260-280nm wavelength and 1 μg of RNA was reverse transcribed using the cDNA synthesis kit (cDNA Synthesis Kit, Bio-Rad, Hercules, CA). The reverse transcribed cDNA products were amplified using a TaqMan Gene Expression Assays kit (Applied Biosystems). This kit contains SphK1 primers and FAM dye-labeled probes and had been tested and optimized for the analysis of mice SphK1 mRNA expression by the manufacturer. A TaqMan gene expression assays kit for detecting the levels of 18S rRNA was used as an endogenous control. Data were gathered and analyzed by the same real-time PCR detection system. The cycle threshold (Ct) values were exported into a Microsoft Excel worksheet for calculation of gene expression in accordance with the ΔΔCt method. The Ct values were first normalized with respect to 18S rRNA levels to obtain ΔCt values. The ΔCt values for SphK1 from the kidney tissue of wild type control group were used as a reference to calculate ΔΔCt values for all other samples. Relative mRNA levels were expressed as $2^{-\Delta\Delta Ct}$.

2.3 Protein preparation and Western Blot

Renal tissues were homogenized with a glass homogenator in ice-cold RIPA lysis buffer containing: 150 mM NaCl, 1.0% IGEPAL® CA-630, 0.5% sodium deoxycholate, 0.1% SDS, 50 mM Tris, protease inhibitor (1:50), pH 8.0. After centrifugation of the homogenate at 5000g for 5 minutes at 4°C, the supernatant was collected and transferred into a new microtube. The measurement of protein concentration was performed using Bradford

Assay. The dye reagent was prepared by diluting 1 part Dye Reagent Concentrate (Bio-Rad Protein Assay Dye Reagent Concentrate) with 4 parts distilled, deionized (DDI) water. Diluted dye reagent was filtered to remove particulates. Three serial dilutions of a protein standard were prepared and Bovine Serum Albumin (BSA) is as standard. The linear range of the assay for BSA is used as 0.2 to 0.9 mg/ml. Pipet 100 μl of each standard and sample solution into a clean, dry test tube. Protein solutions were assayed in duplicate. Add 5.0 ml of diluted dye reagent to each tube and vortex. The mixtures were incubated at room temperature for at least 5 minutes. Finally, the protein concentration was determined by the absorbance at 595 nm in disposable polystyrene cuvettes with 1 cm path length by Shimadzu UV160U UV-Visible Recording Spectrophotometer. The protein samples were frozen in liquid nitrogen and stored at −80°C until used. Western blot analyses were performed as described previously [78]. In brief, kidney tissue protein (15 μg) was subjected to 10% SDS-PAGE, transferred onto a PVDF membrane and blocked by solution with 5% non-fat dry milk in TBS-T. Primary antibodies used in the present study included GAPDH (rabbit 1:3000, Cell Signaling Technology), collagen I/III (rabbit 1:2000, Calbiochem), and α-smooth muscle actin (α-SMA) (rabbit 1:2000, Abcam) and PVDF membrane was incubated in incubation box with primary antibody overnight in 4°C cold room. After the incubation, membrane was washed with TBS 3 times and 10 minutes each time. After washed, PVDF was incubated with horseradish peroxidase (HRP) conjugated secondary antibody goat anti-rabbit (1:2000, Santa Cruz Biotechnology) for 1 hour and then washed with TBS 3 times and 10 minutes each time. Remove all TBS from incubation box, and mix 500μl Luminol enhancer solution (Thermo Fisher Scientific) with 500μl Peroxide solution (Thermo Fisher Scientific) and then

incubation box was swung by swing bed for 1 minute. Membrane was detected by Odyssey® Fc Imaging System (LI-COR®) with 2 minutes exposure time. The intensities of the blots were determined using an imaging analysis program (Image J, free download from http://rsbweb.nih.gov/ij/). The intensities of target protein α-SMA and collagen I/III were divided by the intensities of loading control (GAPDH) to obtain the 1st ratio value. This gave the average target protein value for the WT-C. Then 1st ratio value for each group was divided by the average target protein value of WT-C to obtain the 2nd ratio value. The 2nd ratio values were used to normalize the intensity of the target protein band for each group by averaging the 2nd ratio value for each group.

2.4 Immunohistochemistry

Kidney tissue sections (5 µm) embedded in paraffin were cut and mounted onto microscope slides. Deparaffinization was induced through heat, tissue cleaning agent, ethanol and water. To unmask antigen binding sites, slides were boiled in 0.01 M citrate buffer pH 6.0 for 20 min. Endogenous peroxidase activity was blocked by incubating slides in 3% H_2O_2 in 100% MeOH for 30 min. The sections were then incubated at room temperature for 30 min in 10% Bovine Serum Albumin (BSA) to block nonspecific binding and incubated overnight at 4 °C in a humid chamber with antibodies against α-SMA (1:300, Abcam), CD43 M-19 (1:100, Santa Cruz Biotechnology) and CD68 KP-1 (1:100, Santa Cruz Biotechnology) diluted in PBS-T buffer. Then, after the washing, the slides were incubated for 30 min at room temperature in a humid chamber with a biotinylated goat anti-rabbit IgG-B antibody (1:300, Santa Cruz Biotechnology), donkey anti-goat IgG-B (1:200, Santa Cruz Biotechnology) or goat anti-mouse IgG-B (1:200, Santa Cruz Biotechnology) diluted in PBS-T. The slides were subsequently placed in streptavidin-

horseradish peroxidase for 30 min at room temperature in a humid chamber. Finally, the slides were incubated with 50 µL of diaminobenzidine (BioGenex, San Ramon, CA) as a substrate, counterstained with hematoxylin (Sigma-Aldrich, Saint Louis, MO), dehydrated, and fixed with Permount histological mounting medium (Fisher Scientific, Hampton, NH).

Collagen I/III was stained using picro sirius red. Sirius red is a strong anionic dye, which react with amino group of lysine and hydroxylysine, and the guanidine groups of arginine via its sulphonic acid groups. In addition, Picrosirius appeared to be selective for collagen and however, the reason is unknown [79]. Deparaffinization was the same as immunohistochemistry. Two solutions were prepared before staining. Solution A is Sirius red F3B (C.I. 35782) 0.5g with saturated aqueous solution of picric acid 500ml. Solution B is acidified water containing 5ml acetic acid in 1 liter of distilled water. After deparaffination, slides were stained with hematoxylin (Sigma-Aldrich, Saint Louis, MO) for nuclear staining and then solution A for one and half hour. The solution A on the sections was washed off with two changes of solution B. Different with immunohistochemistry, Sirius Red staining was dehydrated in three changes of 100% ethanol and fixed with Permount histological mounting medium (Fisher Scientific, Hampton, NH) also.

The percentage of collagen positive-stained area was calculated using a computer program Image-Pro Plus 6.0 in 5 microscopic x200 magnification photomicrographs for each group. **Figure 3** describes how to analyze the percentage of positive-stained area:

Firstly, choose class 1 color shown in red to mark the positive-stained area and then add another class color shown in yellow to mark the tissue area and press count. Finally, the program gives us the percentage of each area. However, we tried two methods to analyze the immunohistochemistry of CD43 and CD68 staining. First method utilized percentage of positive-stained area in 5 microscopic x200 magnification photomicrographs for each group, which is also the same as quantification of percentage of collagen-stained area. Second method as shown in **Figure 4**, utilized cell counter by Image J program in 5 microscopic x400 magnification (around 100 cells) photomicrographs for each group. After results were obtained by the two methods, the results were normalized using Microsoft Excel. The percentage of positive-stained area or percentage of the number of positive-stained cells were divided by the average of WT-C in each group each time to get the 1st ratio. The 1st ratio values were used to normalize the percentage of positive-stained area or percentage of the number of positive-stained cells by averaging the 1st ratio values for each group. The results were presented as fold change normalized with the WT-C.
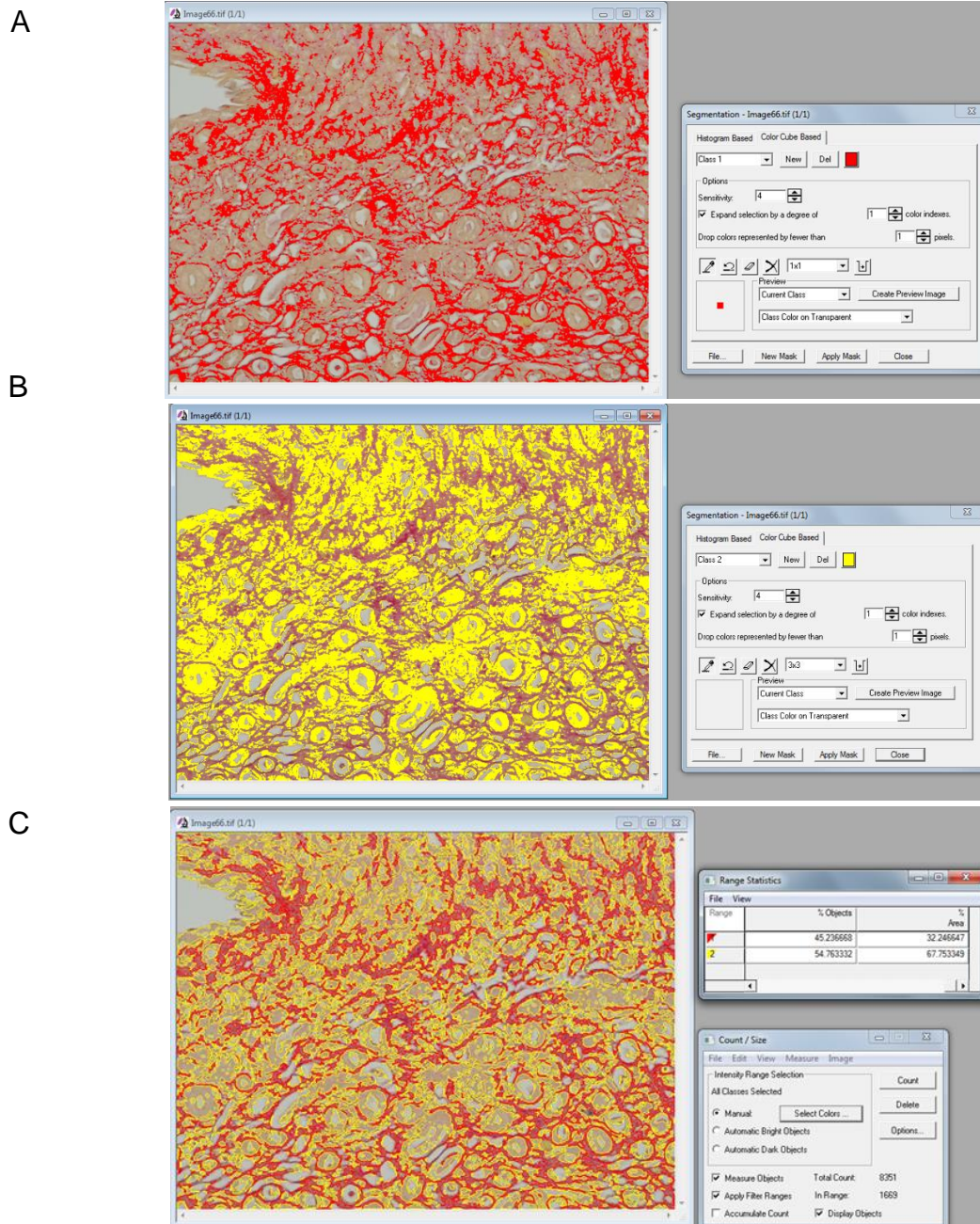
Figure 3. Semiquantification of positive staining area from Sirius Red staining by Image-Pro Plus. A: Choose class 1 color shown in red to mark positive staining area. **B:** Choose class 2 color shown in yellow to mark staining of tissue area. **C:** Press count and the program will show the percentage of each staining area.
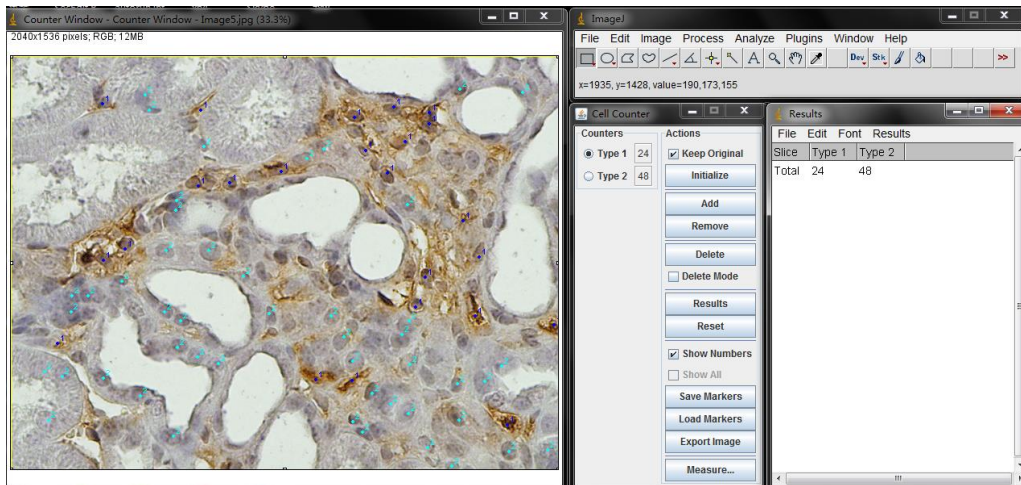
Figure 4. Semiquantification of positive cell staining from immunohistochemistry by cell counter in Image J. Type 1 shows the number of positive staining cells and Type 2 shows the number of normal tissue cells. Percentage of number of positive staining cells was calculated using the following equation: Percentage of the number of positive staining cells = Type 1 / (Type 1 + Type 2)

2.5 Morphological examinations

Glomerular and tubular structures were examined using fixed paraffin-embedded kidneys, stained with Periodic-Acid Schiff (PAS) stain (SIGMA-ALDRICH PAS staining system). First, kidney tissue section were deparaffinized and hydrated in deionized water and then immersed in Periodic Acid Solution for 5 minutes at room temperature. Periodic Acid Solution was rinsed off in distilled water. Next, slides were immersed in Schiff's reagent for 15 minutes at room temperature and then rinsed in running tap water for 5 minutes. Finally, sildes were counterstained in Hematoxylin (Sigma-Aldrich, Saint Louis, MO) for 90 seconds and then rinsed with tap water for 5 minutes. Sections were dehydrated and fixed with Permount histological mounting medium (Fisher Scientific, Hampton, NH). Glomerulus and tubules were scored on a scale of 0–4 depending on the extent of sclerotic changes. Tubular injury score and glomerular damage index were scored semiquantitatively by two blinded manners on the minimum 50 cortical fields of PAS staining using ×400 magnification. The tubular injury is defined as tubular dilatation, tubular atrophy, sloughing of tubular epithelial cells, or thickening of the tubular basement membrane and the glomerular damage is defined as segmental or global capillary collapse with increased matrix deposition. The score was calculated on a scale of 0 to 4, as follows: 0 = no injury; 1 = 1–25% injured area; 2 = 26–50% injured area; 3 = 51–75% injured area; 4 >75% injured area [80-82].

2.6 Statistical Analyses

Data are expressed as the mean ± standard error of the mean (SEM). Comparisons among groups were performed with two-way analysis of variance (ANOVA) followed by

Dunnett's test to examine the effects of gene deletion and UUO treatment as the independent factors. $P < 0.05$ was considered statistically significant.

CHAPTER THREE

RESULTS

3.1 Attenuated renal interstitial fibrosis induced by UUO in SphK1 KO mice

3.1.1 Enhanced expression of SphK1 mRNA in UUO model

To determine the effect of UUO model and SphK1 KO on the expression of SphK1 mRNA level, real time RT-PCR was performed on kidney RNA from Day 7 UUO mice. As shown in **Figure 5**, the relative expression of SphK1 mRNA was significantly increased in WT-UUO compared with WT-C whereas it was barely detectable in KO-UUO compared with WT-UUO. It is suggested that the UUO induces expression of SphK1 mRNA, which is prevented in SphK1 KO mice.
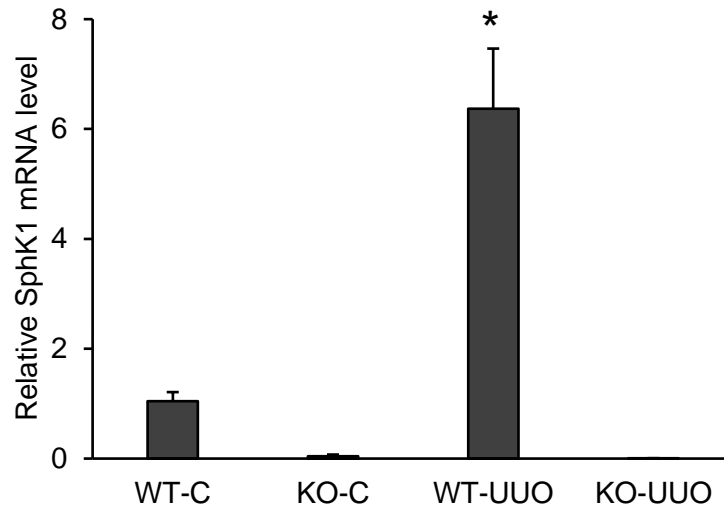
Figure 5. Effect of UUO and SphK1 KO on SphK1 mRNA levels: Real time RT-PCR analysis showing relative SphK1 mRNA levels in different groups. The final results were presented as fold change normalized with the WT-C. Data are presented as the mean ± SEM. * $P< 0.05$ vs. WT-C (n =3-4), Day 7 UUO.

3.1.2 No significant difference in the induced expression of fibrotic markers in Day 7 UUO model between WT and SphK1 KO mice

To detect whether renal fibrosis induced by UUO was attenuated in SphK1 KO mice, western blot was performed on Day 7 UUO mice first. **Figure 6A** shows representative western blot images depicting the levels of collagen I and α-SMA with GAPDH as loading controls. In summarized intensities as shown in **Figures 6B** and **6C**, levels of α-SMA were increased in WT-UUO and KO-UUO, and there was statistic significantly attenuated in KO-UUO compared with WT-UUO. In addition, levels of collagen I were also increased in WT-UUO and there was statistic significant difference between WT-UUO and KO-UUO. However, the decrease level of these two fibrotic markers in SphK1 knockout UUO group compared with WT-UUO is not that much, which drove us to move to Day 14 UUO model.
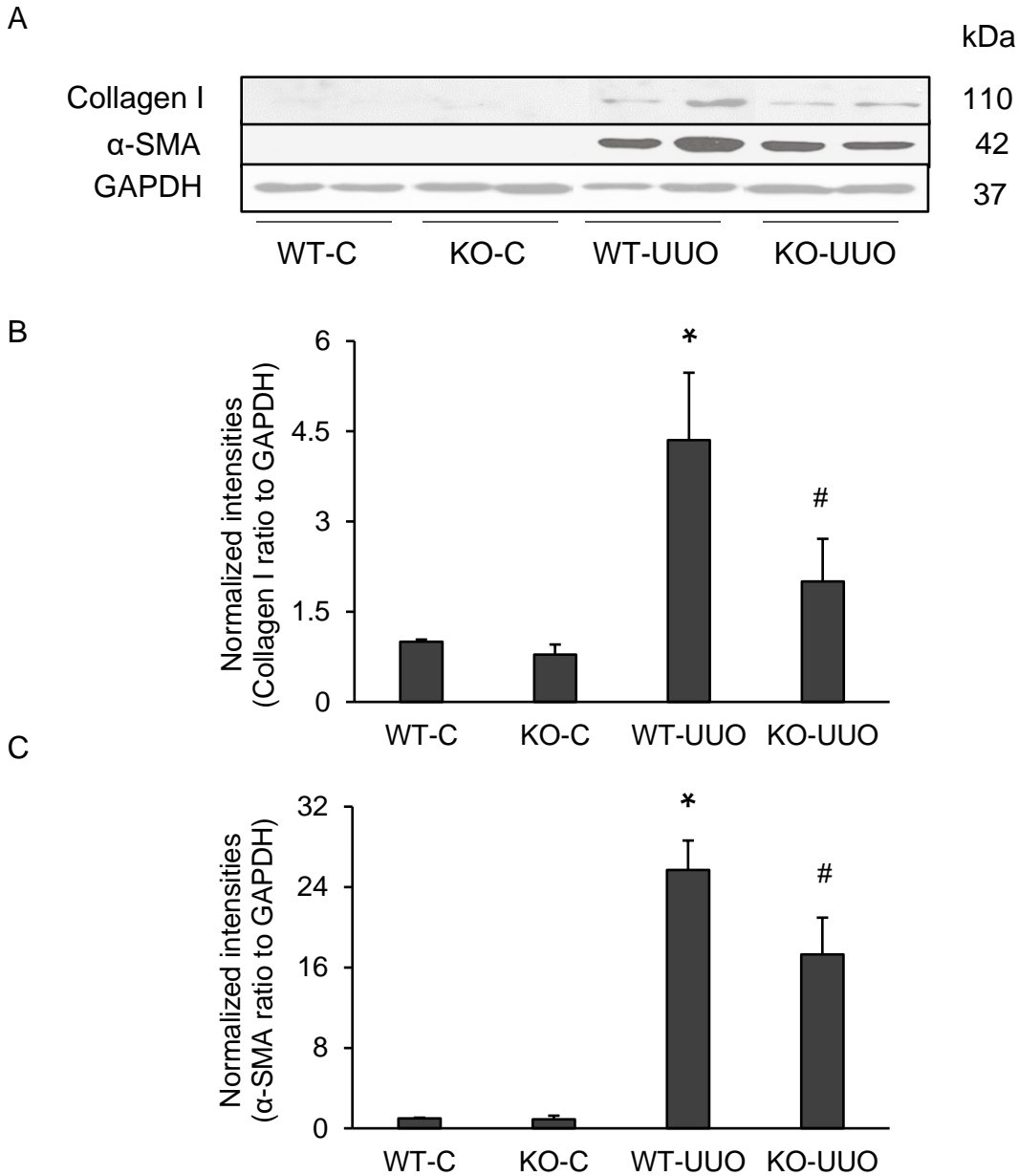
Figure 6. Effect of UUO and SphK1 KO on the expression of fibrotic markers in Day 7 UUO model. A: Representative gel documents showing α-SMA (42 kDa) and Collagen I (110 kDa) levels. **B:** Summarized data showing the levels of collagen I quantitated as a ratio of detected specific protein band vs. GAPDH as loading control (n=5). **C:** Summarized data showing the levels of α-SMA quantitated as a ratio of detected specific protein band vs. GAPDH as loading control (n=5). The final results were presented as fold change normalized with the WT-C. Data are presented as the mean ± SEM. * p ＜0.05 vs. WT-C; # p ＜0.05 vs. WT-UUO (n=5), Day 7 UUO.

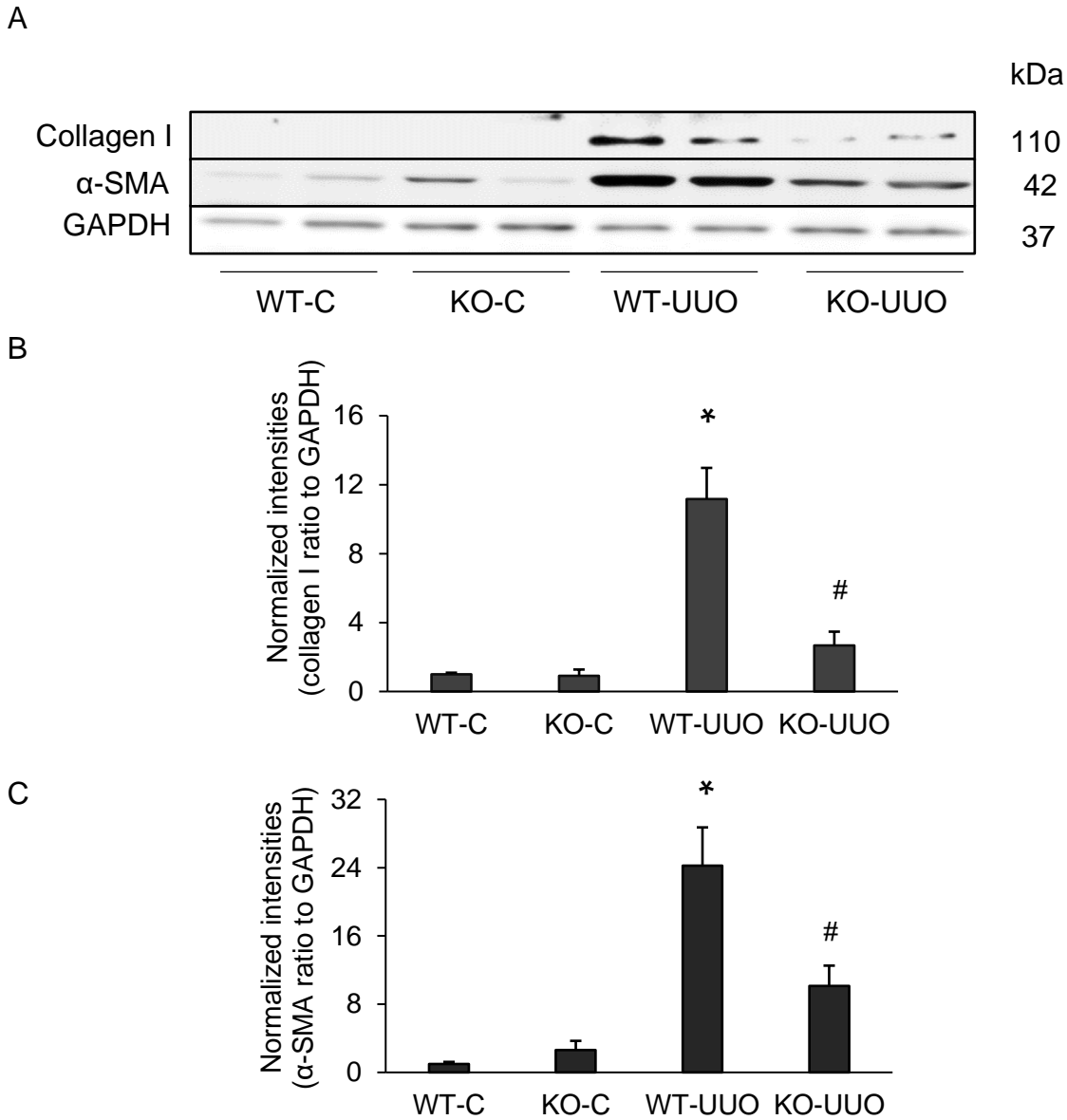### 3.1.3 Attenuated expression of fibrotic markers in SphK1 KO mice Day 14 UUO model

To detect whether renal fibrosis induced by UUO was attenuated in SphK1 KO mice, western blot was performed on Day 14 UUO mice. **Figure 7A** shows representative western blot images depicting the levels of collagen I and α-SMA with GAPDH as loading controls. In summarized intensities as shown in **Figures 7B** and **7C**, levels of α-SMA and collagen I were significantly increased in WT-UUO and KO-UUO, whereas the levels of α-SMA and collagen I were significantly reduced in KO-UUO compared with WT-UUO. It is suggested that the deletion of SphK1 inhibits fibrogenesis in UUO-induced renal fibrosis.

A

B

C

Figure 7. Effect of UUO and SphK1 KO on the expression of fibrotic markers in Day 14 UUO model. A: Representative gel documents showing α-SMA (42 kDa) and collagen I (110 kDa) levels. **B:** Summarized data showing the levels of collagen I quantitated as a ratio of detected specific protein band vs. GAPDH as loading control (n=6). **C:** Summarized data showing the levels of α-SMA quantitated as a ratio of detected specific protein band vs. GAPDH as loading control (n=6). The final results were presented as fold change normalized with the WT-C. Data are presented as the mean ± SEM. * p $<$ 0.05 vs. WT-C; # p $<$ 0.05 vs. WT-UUO (n=6), Day 14 UUO.

3.1.4 Distribution of fibrotic marker α-SMA in renal interstitial space

To further detect renal interstitial fibrosis induced by UUO, we used immunohistochemistry for α-SMA staining on Day 7 UUO mice. The positive α-SMA staining showed a brown color in photomicrographs. As shown in **Figure 8**, in 100x magnification of the photomicrographs, the distribution of α-SMA was mainly located in outer medulla and renal cortical area and that there was almost no staining in inner medulla; in 200x magnification of photomicrographs, it was more clearly visible that the distribution of α-SMA in the renal interstitial area. These results suggest that the elevated expression of α-SMA induced by UUO is located in renal interstitial space.
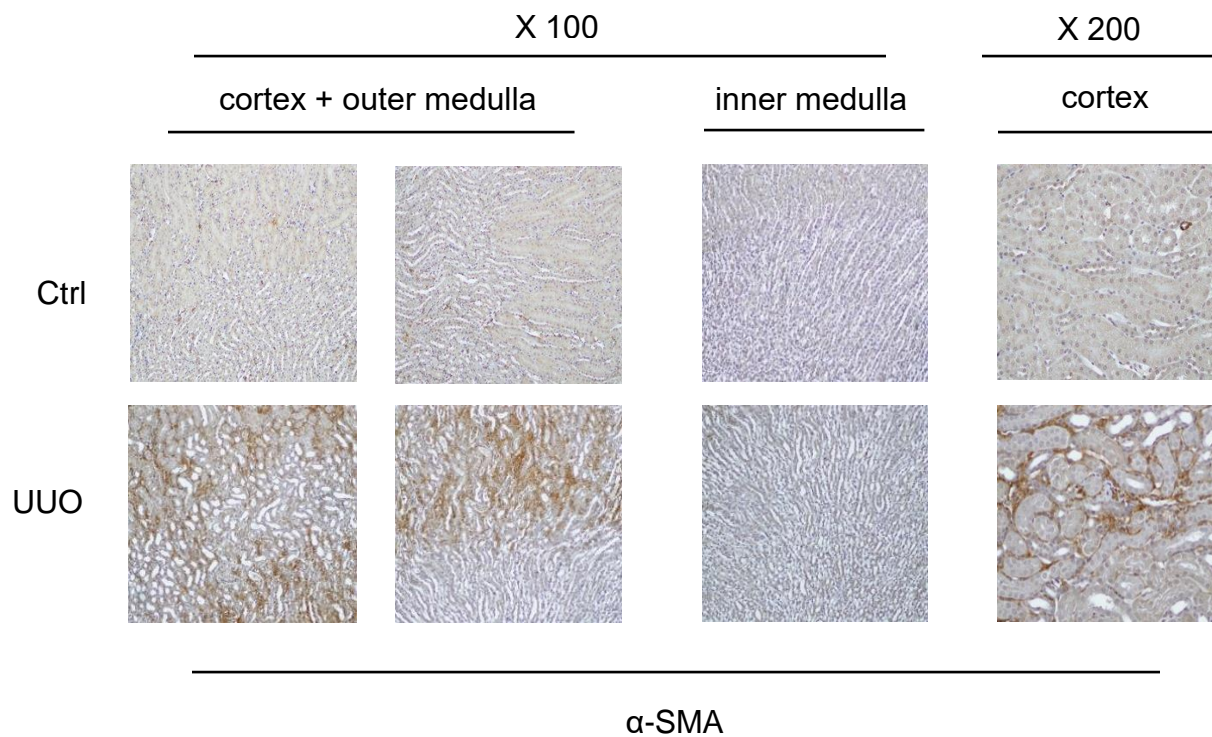
Figure 8. Effect of UUO on α-SMA distribution in kidneys. Immunostaining of α-SMA was applied on Day 7 UUO mice in WT-UUO and WT-C. The brown color indicates positive staining in cortex, outer medulla and inner medulla, respectively.

3.1.5 Distribution of extracellular matrix protein collagen in renal interstitial space and less collagen staining in SphK1 KO mice

To further detect whether UUO induced renal interstitial fibrosis and knockout of SphK1 inhibited fibrogenesis, we used Sirius Red staining, which is a staining specific to collagen [83], on Day 14 UUO. As shown in **Figure 9A**, in 400x magnification of photomicrographs, the collagen positive staining area in red color and that the collagen staining area was mainly located in renal cortical interstitial area. Summarized percentage of collagen staining area is shown in **Figure 9B**. The collagen staining area was notably more in UUO groups than in control groups, but much less in KO-UUO than in WT-UUO, which was consistent with the result of western blot analysis. These data indicate that renal interstitial fibrosis induced by UUO is attenuated in SphK1 KO mice.

A

B
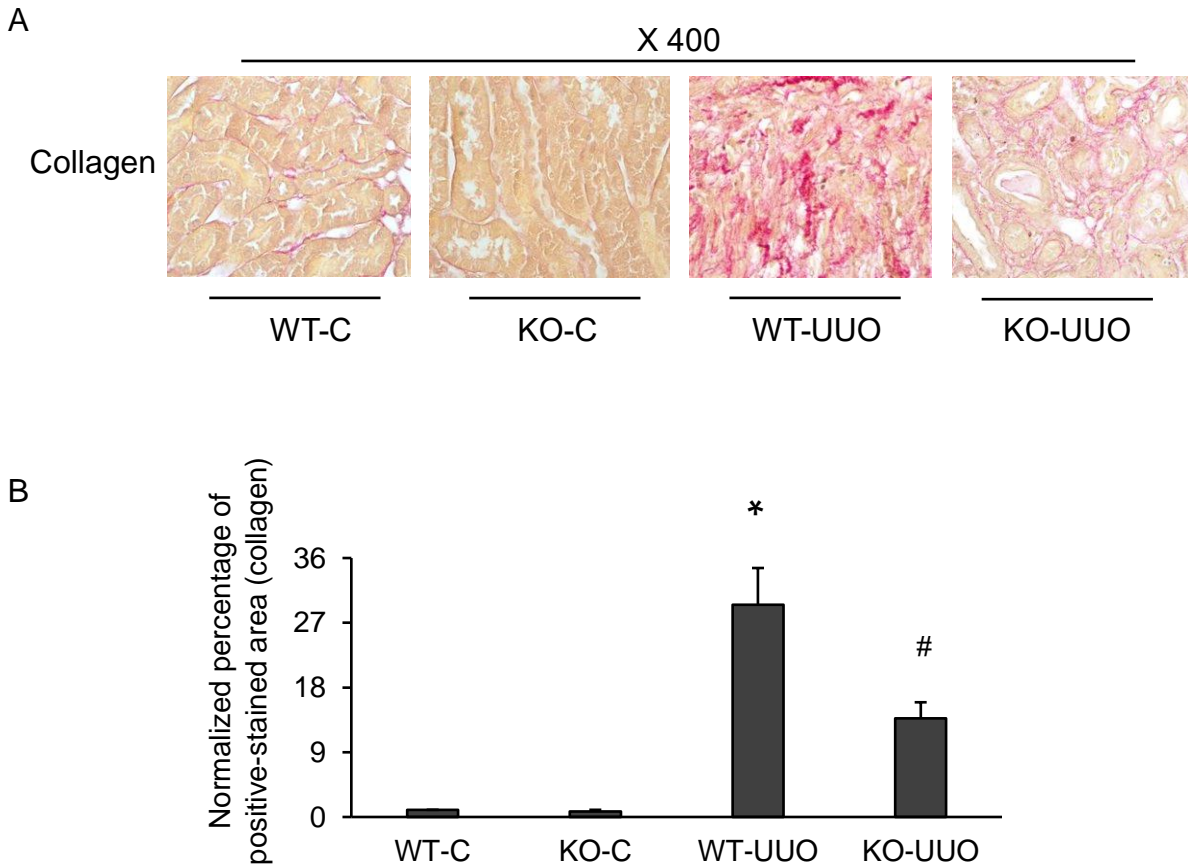
Figure 9. Effect of UUO and SphK1 KO on collagen distribution by Sirius Red staining. A: Representative pictures of Sirius-Red-stained kidney sections in cortical area and the positive collagen staining area showing red color in 400x magnification of photomicrographs. B: The average percentage of collagen staining was quantified by analyzing at least five random fields in x200 magnification of photomicrographs per kidney sample using Image-Pro Plus software. The final results were presented as fold change normalized with the WT-C. Data are presented as the mean ± SEM. * p ＜0.05 vs. WT-C; # p ＜0.05 vs. WT-UUO (n=5), Day 14 UUO.

3.2 No significant difference in the infiltration of immune cells between WT-UUO and KO-UUO

As mentioned above, SphK1-S1P-S1PRs axis is also involved in immune regulation and that one of the 5 stages of renal fibrosis is infiltration of immune cells into damaged tissue, which further regulates fibrogenesis. We wanted to detect whether the changes in renal fibrotic markers between WT-UUO and KO-UUO were due to the immune regulation by KO of SphK1. CD43, T-cell marker, and CD68, macrophage marker, which indicated immune response, were stained with immunohistochemistry and the representative positive staining area was shown brown color in 200x magnification of photomicrographs. As shown in **Figure 10A**, the infiltrated immune cells were also mainly located in interstitial area. **Figures 10B and 10C** show the normalized average percentage of CD43- and CD68- positive cells. The positive staining cells were notably more in WT-UUO and KO-UUO than those in WT-C and KO-C, but there was no significant difference between WT-UUO and KO-UUO. **Figures 10D and 10E** show the normalized average percentage of CD43- and CD68- positive-stained area. The results were consistent with normalized average percentage of CD43- and CD68- positive cells. These two methods of analysis of immune cells infiltration indicate that the difference in renal fibrotic markers between WT-UUO and KO-UUO may not be due to the possible immune regulation by SphK1 deletion, rather the direct effect of SphK1 deletion on kidney tissue.

A
X 200

CD43-

CD68-

WT-C   KO-C   WT-UUO   KO-UUO

B

C
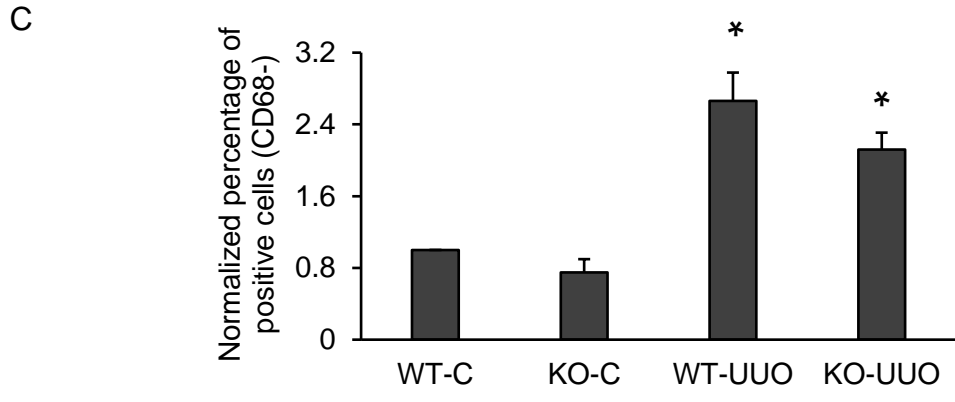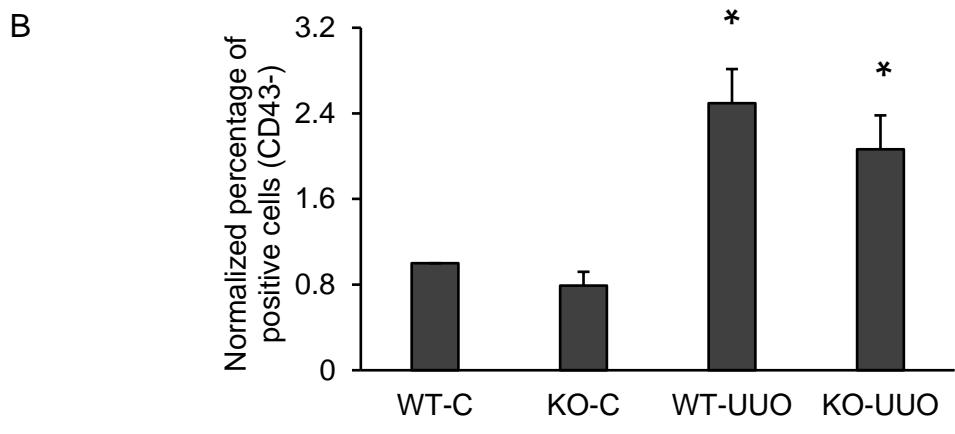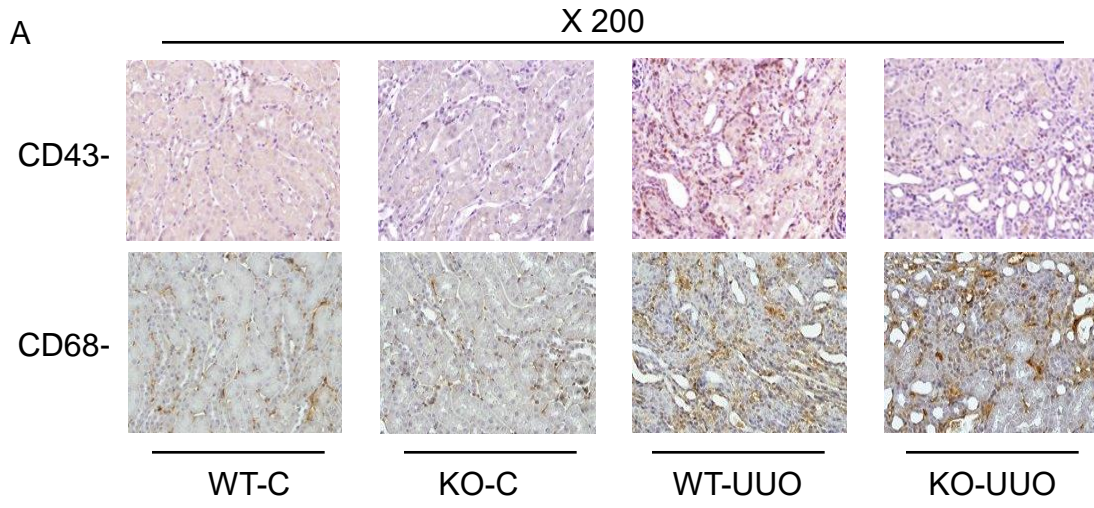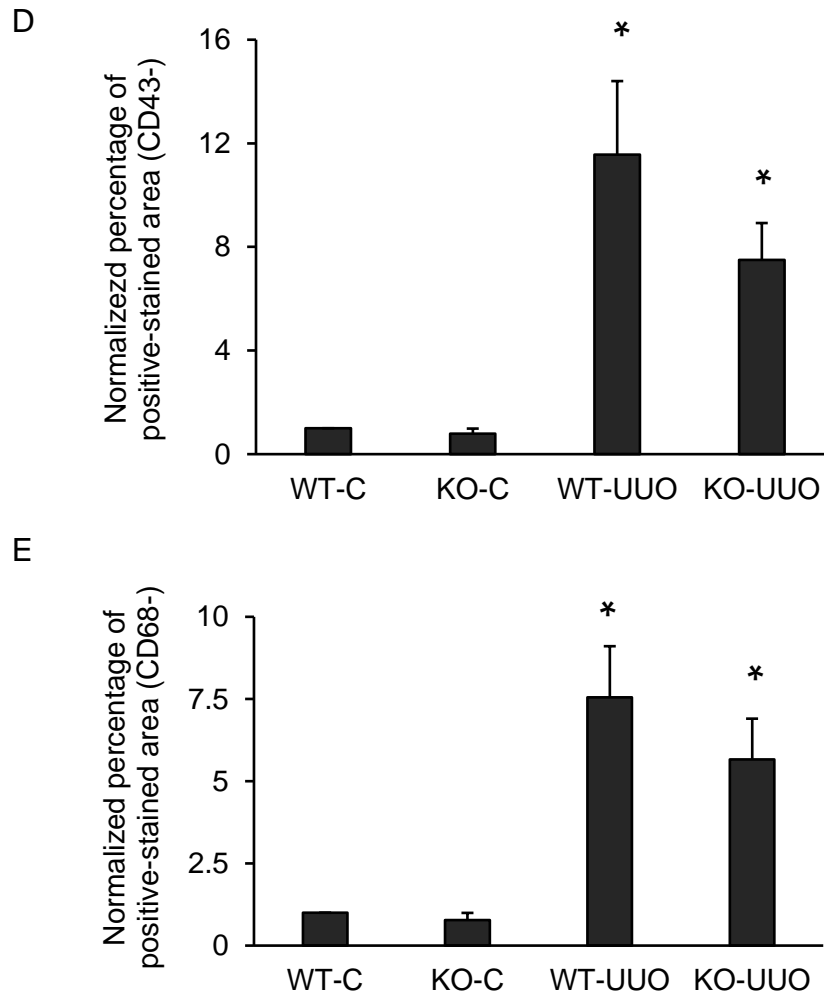
Figure 10. Effect of UUO and SphK1 KO on the infiltration of immune cells. A: Representative photomicrographs of immunohistochemistry of kidney sections in cortical area and the CD43- and CD68- positive cells staining showing brown color in 200x magnification of photomicrographs. **B, C:** The percentage of CD43- and CD68- positive cells was quantified by analyzing at least five random fields in 400x magnification of photomicrographs per kidney sample with Image J. **D, E:** The percentage of CD43- and CD68- positive area was quantified by analyzing at least five random fields in 200x magnification of photomicrographs per kidney sample with Image-Pro Plus software. The final results were presented as fold change normalized with the WT-C. Data are presented as the mean ± SEM. * $p < 0.05$ vs. WT-C (n=5), Day 14 UUO.

3.3 Attenuated morphological injury induced by UUO in SphK1 KO mice

To detect whether knockout of SphK1 was protective against kidney damage induced by UUO, the morphological injury was evaluated for glomerular damage index and tubular injury score on PAS staining. As shown in **Figure 11A**, glomeruli and tubules in UUO tissue showed a typical pathological damage profile. There was exhibiting expanded mesangial matrix with hypercellularity, capillary collapse, and fibrous deposition in the glomeruli and tubular atrophy and vacuolar degeneration in the tubule epithelia. The two blinded manners selected minimum 50 renal cortical areas to score tubular injury and glomerular damage. Summarized tubular injury scores and glomerular damage indices were shown in **Figures 11B** and **11C.** The injury scores were notably higher in WT-UUO and KO-UUO than that in WT-C and KO-C respectively, but much lower in KO-UUO than that in WT-UUO. It is suggested that UUO induces kidney damage through glomerular damage and tubular injury and compared with wild type mice, knockout of SphK1 protects kidney in the UUO model.
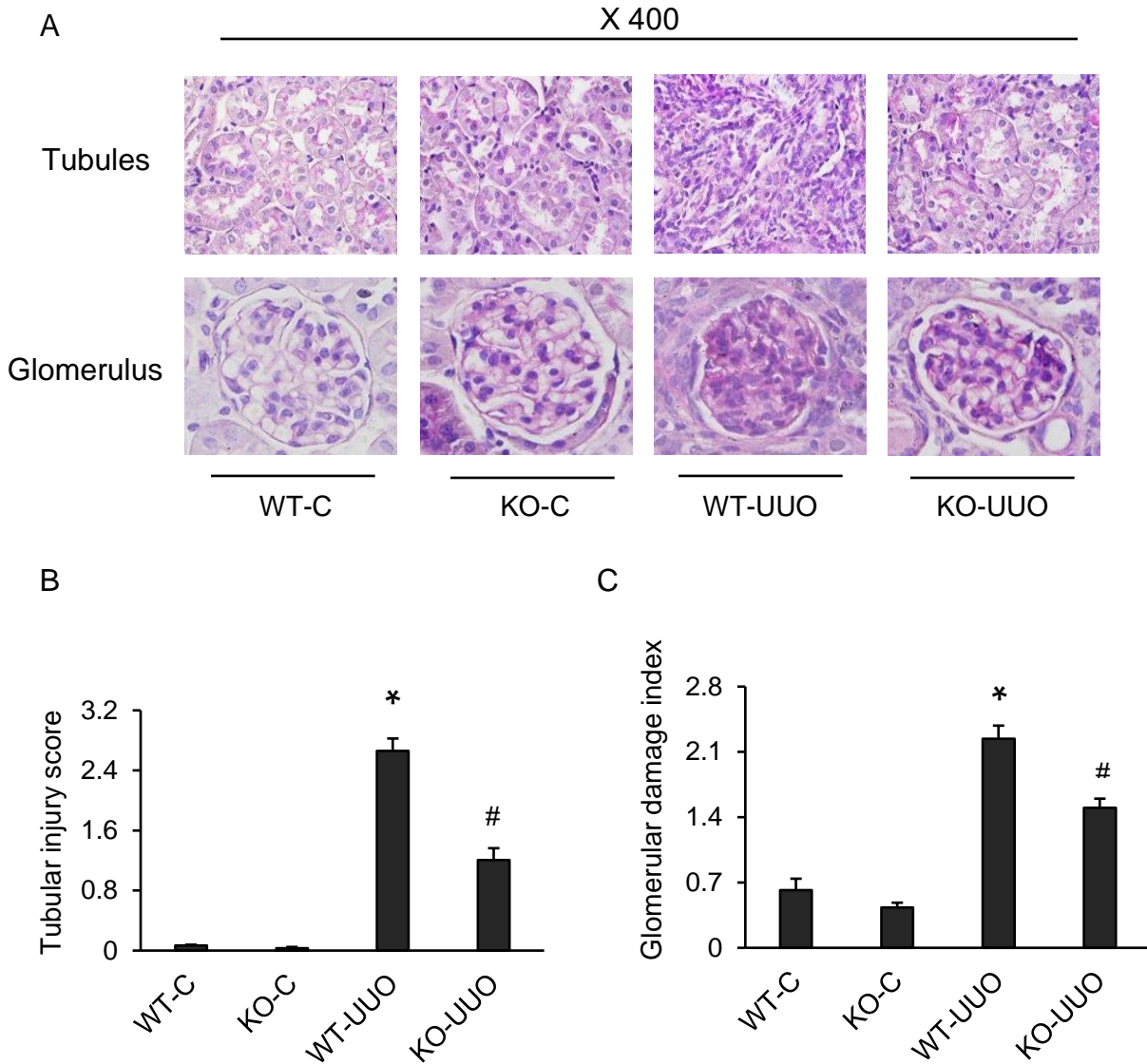
Figure 11. Effect of UUO and SphK1 KO on kidney damage. A: Representative photomicrographs showing tubular and glomerular structures [Periodic Acid-Schiff (PAS) staining, ×400]. **B, C:** Summarized tubular injury score and glomerular damage index by semiquantitation of scores in different groups. The final results were presented as fold change normalized with the WT-C. Data are presented as the mean ± SEM. * p ＜0.05 vs. WT-C; # p ＜0.05 vs. WT-UUO (n=5), Day 14 UUO.

CHAPTER FOUR

DISCUSSION AND CONCLUSION

Since there was considerable evidence showing that the SphK1/S1P/S1PRs axis was involved in various organ fibroses as mentioned in the introduction, the major goals of the our study were to determine whether SphK1/S1P signaling mediated renal interstitial fibrosis induced by UUO and if deletion of SphK1 in mice attenuated renal interstitial fibrosis *in vivo* study. To induce renal interstitial fibrosis we applied UUO model on male mice. The reason for selecting male mice is that female mice are resistant to renal interstitial fibrosis induced by UUO [84]. Furthermore, it has been found that there is a higher rate for CKD in men than in women due to hormonal regulation between males and females [85]. If we tested our hypothesis in female mice, it would take more time to build UUO model than if we used male mice referring to the results from **Figure 6** and **Figure 7**. Furthermore, we were not sure if SphK1/S1P also participated in hormonal regulation to further mediate renal interstitial fibrosis. For those reasons, we decided to choose male mice to test our hypothesis.

At first, we observed that the expression of SphK1 mRNA was increased 6.1 fold in WT-UUO compared with WT-C in Day 7 UUO model. This observation suggested that upregulated SphK1 might participate in the renal injury. Interestingly, the increased level of SphK1 was consistent with the findings from a previous study [86], which utilized SphK1 transgenic (TG) mice that overexpressed SphK1, to detect if SphK1/S1P/S1PRs mediated fibrogenesis. That study showed that in SphK1 TG mice, the elevated SphK1 increased the production of S1P and then initiated spontaneous generation of interstitial and perivascular cardiac fibrosis in 3 month old SphK1 TG mice. In addition, deletion of S1PR3 attenuated cardiac fibrosis in SphK1 TG mice [86]. Our observation of induced level of SphK1 together with the mentioned findings by others strongly indicate that SphK1/S1P/S1PRs participates in the renal fibrogenesis in CKD. We then went on further examine whether the endogenous change of SphK1 in a disease model really participated in CKD.

Secondly, to detect whether SphK1/S1P signaling mediated renal fibrosis in the UUO model we identified the levels of fibrotic markers in mice with SphK1 deletion and based on these markers, we found that renal fibrosis induced by UUO was considerably attenuated in SphK1 KO mice **(Figure 7)**. As mentioned above, S1P is involved in different types of fibrosis and one of the previous studies has reported that the endogenous S1P in liver tissues is increased in cholestasis-induced liver fibrosis [87]. We assumed that UUO model may induce renal fibrosis by elevating level of S1P in kidney by SphK1. Consistent with a previous study, it has been shown that exogenous S1P induces fibrogenesis in NRK49F cells *in vitro* [88]. In that study, the expression of

α-SMA, collagen I, collagen IV, tissue inhibitor of metalloproteinase-1 (TIMP1) and plasminogen activator inhibitor-1 (PAI1) and the activity of cell migration were increased and the expression of E-cadherin was decreased in the S1P-stimulated NRK49F (normal rat kidney fibroblast cells) cells. In addition, the changing levels of these markers were related to gradient doses of S1P. That study also showed that renal fibrosis, interstitial injury and the activity of cell migration were decreased in UUO model by antagonism of S1PRs with nonselective functional antagonist FTY720 and by inhibiting sphingosine kinases by DMS, a sphingosine kinase inhibitor, *in vivo*. It introduced exogenous compounds to detect the effect of fibrogenesis on UUO model [88]. However, we detected the effect of endogenous SphK1 on UUO model, which identified the role of endogenous SphK1 in UUO-induced fibrosis. Our findings led to the conclusion that SphK1/S1P/S1PRs mediated renal fibrosis in UUO model. Other investigators applied different days of UUO model depending on the stage of renal fibrosis they studied. Our data from Day 7 UUO model **(Figure 6)** did show the statistic difference between WT-UUO and SphK1 KO-UUO, but the reduction in the levels of fibrotic markers in Day 7 KO-UUO group is not significant compared with Day 14 UUO model. However, we manipulated the UUO surgery on Day 7 and Day 14 in different time course. Probably, the effect of day length of UUO model and genetic interaction on renal fibrosis need to be investigated in future with identical time course of UUO surgery.

It should be noted that the protein levels of fibrotic markers are still significantly higher in SphK1 KO UUO group than in non-UUO groups, which indicates that there may be a compensation of S1P produced by SphK2 in SphK1 KO mice. In addition, it cannot be

ruled out that there may be other S1P-independent signaling pathways contributing to fibrogenesis in UUO model. Indeed, our previous studies have shown that prolyl hydroxylase (PHD)/hypoxia-inducible factor (HIF)-1α signaling mediates fibrogenesis induced by TGF-β [89]. As a result, there may be interactions between S1P signaling pathway and other pathways in renal fibrosis, which remains to be clarified.

As we mentioned above, S1P as a bioactive molecule can initiate both extracellular and intracellular pathways. We assumed that S1P as a mediator of fibrosis may act through targeting its receptors and receptor-independent signaling to mediate fibrogenesis. One of the previous studies has found that S1P induces liver fibrosis without binding to S1PRs [90] . That study has reported that the exogenous TGF-β through increasing expression of SphK1 induces the elevation of expression of collagen I and collagen III, which cannot be attenuated in the presence of S1PRs antagonists. It is assumed that SphK1/S1P has its own intracellular signaling pathway to regulate fibrogenesis [90]. Our study did not detect which subtypes of receptors were involved in renal interstitial fibrosis induced by UUO, which is worth investigating in future study.

In addition to measuring the levels of the fibrotic markers by western blot analyses, we also performed fibrotic markers staining in tissue. In our findings, UUO induced renal interstitial fibrosis according to the distribution of collagen and α-SMA staining shown in **Figure 8** and **Figure 9**. We did both Day 7 and Day 14 UUO model to detect distribution of collagen and α-SMA. Surprisingly, the quantified collagen positive-stained area in Day 14 UUO model was consistent with western blot, whereas the result of α-SMA staining

in Day 14 UUO showed no significant difference between SphK1 KO UUO and WT-UUO after normalizing the percentage of positive-stained area. The explanation of this phenomenon is that in Day 14 UUO model, the tubular dilatation, atrophy and loss of tubular epithelial cells reached the end stage and the distribution of α-SMA expressed in mesenchymal cells would be affected by cell loss [91] and further affect the result of protein staining. Thus, the results of α-SMA from protein levels by western blot and the distribution by immunostaining were different.

Then we detected the distribution of α-SMA by immunohistochemistry on Day 7 UUO model, in which the structure of UUO kidney remained relatively intact. We found that α-SMA and collagen positive-stained area in UUO kidney was mainly located in cortical interstitial area. One of the previous studies has reported that HIF-1α not only is the consequence of renal interstitial fibrosis but also is an inducer to mediate EMT in CKD and the genetic deletion of HIF-1α attenuates the expression of fibrotic markers such as α-SMA and connective tissue growth factors (CTGF) [92]. It is suggested that besides the elevation of HIF-1α as one of the outcomes of fibrosis, HIF-1α is also an important regulator of fibrogenesis in UUO model. In addition, medulla is more adaptive in hypoxic condition than cortical area because oxygen tensions are estimated to be about 30 mm Hg in cortex and 10 mm Hg O_2 in medulla [93]. As a consequence, we assumed that renal cortical area will produce more HIF-1α than medulla in hypoxic condition, which results in the observation that collagen I and α-SMA are mainly located in cortex interstitial space. Therefore, we can suppose if there is any link between HIF-1α and SphK1/S1P signaling to induce interstitial fibrosis as our further study.

Immune response is involved in the priming stage of the fibrogenesis. The previous study has shown that the infiltration of T cells that represents adaptive immune response and infiltration of macrophages that represents innate immune response start after four-hour-obstruction. In the first 24 hours, the infiltration of T cells is 10 fold and the infiltration of macrophages is 30 fold compared with normal condition, respectively [94] and inflammatory cells progressively infiltrate into kidney tissue for the next 14 days. Chronically, the cytokines secreted from inflammatory cells trigger infiltration of inflammatory cells and induce expressions of more chemokines, cytokines and growth factors, all of which contribute to activation of myofibroblasts and fibrogenesis [95-99]. Interestingly, it also has been reported that the macrophage suppressor mizoribine attenuates renal interstitial fibrosis induced by UUO [100].

S1P is known to be involved in multiple inflammatory responses such as recruitment of immune cells into injured tissue. It has been reported that extracellular S1P targets S1PRs to initiate downstream signaling pathways and leads to the activation of both STAT3 and NF-κB. STAT3 will further regulate transcription of multiple target genes involving S1PR1 to enhance S1P-S1PR1 signaling pathway. The activated NF-κB upregulates the transcription of proinflammatory cytokines and then induces fibrogenesis [101-104]. Moreover, it is reported that S1P gradients regulate innate and adaptive immune cells trafficking through S1PRs [105]. Given the role of S1P signaling in the regulation of immune response and inflammation, we wondered if SphK1 KO altered the inflammatory process and thereby attenuated fibrosis in UUO. To investigate whether

SphK1/S1P directly acted on renal cells to participate in renal interstitial fibrosis or indirectly via modulating inflammation, our study also detected the infiltration of inflammatory cells in the kidneys with immunohistochemistry **(Figure 10)**. We found that in SphK1 KO UUO, the increased infiltration of inflammatory cells was not significantly different from that in WT-UUO. These results indicate that the SphK1/S1P pathway is probably a direct mediator of renal interstitial fibrosis, rather than immune modulator in the fibrogenesis of UUO. However, there are different phenotypes of macrophages, which present different responsibilities. M1 macrophage is seen as the inflammatory macrophage and M2 is seen as the fibrotic macrophage, so these two phenotypes of macrophage coexist in injury renal to regulate inflammation-mediated renal cell loss and fibrogenesis [106]. To further confirm if SphK1/S1P/S1PRS through mediating inflammatory cells infiltration, the ratio of distribution of different phenotypes macrophages in UUO model need to be identified in future study. In support of our findings, another study using nude mice that were athymic animals with deficiency of T cells found that renal interstitial fibrosis, kidney injury and activity of cell migration induced by UUO in these immune deficient mice could also be significantly attenuated by inhibiting S1P signaling [88, 107]. These reports together with our findings in the present study lead to a conclusion that SphK1/S1P can directly mediate renal interstitial fibrosis through its extracellular pathway in CKD by bypassing the regulation of immune response.

Tubular cell death has a close association with progressive renal interstitial fibrosis and it also has been stated that UUO affects glomerular filtrate rate decreased by 80% and

44

the number of glomerulus reduced by 40%. It can be concluded that UUO contributes to both tubular and glomerular injury [54, 108]. Finally, we detected if UUO and knockout of SphK1 had effect on kidney damage, which was indicated by tubular injury score and glomerular damage index that were the outcomes of UUO **(Figure 11)**. As expected, tubular injury and glomerular damage induced by UUO were attenuated in SphK1 KO mice. The results demonstrate that knockout of SphK1 could be a new strategy to protect kidney structure and renal function from CKD.

In summary, the present study revealed a new triggering mechanism of renal interstitial fibrosis induced by UUO model, which was characterized by upregulation of SphK1 mRNA expression. The deletion of SphK1 attenuated the renal interstitial fibrosis and kidney damage induced by UUO without significant differences in the infiltration of inflammatory cells between WT-UUO and KO-UUO. These results may provide new therapeutic strategies associated with manipulating SphK1/S1P pathway to prevent renal fibrosis and renal failures initiated by CKD or other cardiovascular diseases such as diabetes and hypertension.

REFERENCES

1. Shayman, J.A., *Sphingolipids.* Kidney Int, 2000. **58**(1): p. 11-26.

2. Shayman, J.A. and N.S. Radin, *Structure and function of renal glycosphingolipids.* Am J Physiol, 1991. **260**(3 Pt 2): p. F291-302.

3. Tamama, K. and F. Okajima, *Sphingosine 1-phosphate signaling in atherosclerosis and vascular biology.* Curr Opin Lipidol, 2002. **13**(5): p. 489-495.

4. Liu, H.Y., et al., *Regulation of S1P receptors and sphingosine kinases expression in acute pulmonary endothelial cell injury.* Peerj, 2016. **4**.

5. Pyne, N.J., et al., *Sphingosine 1-phosphate signalling in cancer.* Biochem Soc Trans, 2012. **40**(1): p. 94-100.

6. Maceyka, M. and S. Spiegel, *Sphingolipid metabolites in inflammatory disease.* Nature, 2014. **510**(7503): p. 58-67.

7. Hla, T., *Sphingosine 1-phosphate receptors.* Prostaglandins Other Lipid Mediat, 2001. **64**(1-4): p. 135-42.

8. Liu, H., et al., *Sphingosine kinases: a novel family of lipid kinases.* Prog Nucleic Acid Res Mol Biol, 2002. **71**: p. 493-511.

9. Spiegel, S. and S. Milstien, *Sphingosine 1-phosphate, a key cell signaling molecule.* J Biol Chem, 2002. **277**(29): p. 25851-4.

10. Maceyka, M., et al., *Sphingosine-1-phosphate signaling and its role in disease.* Trends Cell Biol, 2012. **22**(1): p. 50-60.

11. Fyrst, H. and J.D. Saba, *Sphingosine-1-phosphate lyase in development and disease: sphingolipid metabolism takes flight.* Biochim Biophys Acta, 2008. **1781**(9): p. 448-58.

12. Kitatani, K., J. Idkowiak-Baldys, and Y.A. Hannun, *The sphingolipid salvage pathway in ceramide metabolism and signaling.* Cell Signal, 2008. **20**(6): p. 1010-8.

13. Merrill, A.H., Jr. and E. Wang, *Biosynthesis of long-chain (sphingoid) bases from serine by LM cells. Evidence for introduction of the 4-trans-double bond after de novo biosynthesis of N-acylsphinganine(s).* J Biol Chem, 1986. **261**(8): p. 3764-9.

14. Spiegel, S. and S. Milstien, *Sphingosine-1-phosphate: an enigmatic signalling lipid.* Nat Rev Mol Cell Biol, 2003. **4**(5): p. 397-407.

15. Degagne, E. and J.D. Saba, *S1pping fire: Sphingosine-1-phosphate signaling as an emerging target in inflammatory bowel disease and colitis-associated cancer.* Clin Exp Gastroenterol, 2014. **7**: p. 205-14.

16. Newton, J., et al., *Revisiting the sphingolipid rheostat: Evolving concepts in cancer therapy.* Exp Cell Res, 2015. **333**(2): p. 195-200.

17. Maceyka, M., et al., *SphK1 and SphK2, sphingosine kinase isoenzymes with opposing functions in sphingolipid metabolism.* J Biol Chem, 2005. **280**(44): p. 37118-29.

18. Mitra, P., et al., *Role of ABCC1 in export of sphingosine-1-phosphate from mast cells.* Proc Natl Acad Sci U S A, 2006. **103**(44): p. 16394-9.

19. Takabe, K., et al., *Estradiol induces export of sphingosine 1-phosphate from breast cancer cells via ABCC1 and ABCG2.* J Biol Chem, 2010. **285**(14): p. 10477-86.

20.   Kawahara, A., et al., *The sphingolipid transporter spns2 functions in migration of zebrafish myocardial precursors.* Science, 2009. **323**(5913): p. 524-7.

21.   Venkataraman, K., et al., *Vascular endothelium as a contributor of plasma sphingosine 1-phosphate.* Circ Res, 2008. **102**(6): p. 669-676.

22.   Okajima, F., *Plasma lipoproteins behave as carriers of extracellular sphingosine 1-phosphate: is this an atherogenic mediator or an anti-atherogenic mediator?* Biochimica Et Biophysica Acta-Molecular and Cell Biology of Lipids, 2002. **1582**(1-3): p. 132-137.

23.   Pappu, R., et al., *Promotion of lymphocyte egress into blood and lymph by distinct sources of sphingosine-1-phosphate.* Science, 2007. **316**(5822): p. 295-298.

24.   Maceyka, M., et al., *SphK1 and SphK2, sphingosine kinase isoenzymes with opposing functions in sphingolipid metabolism.* Journal of Biological Chemistry, 2005. **280**(44): p. 37118-37129.

25.   Spiegel, S. and S. Milstien, *Sphingosine-1-phosphate: An enigmatic signalling lipid.* Nature Reviews Molecular Cell Biology, 2003. **4**(5): p. 397-407.

26.   Strub, G.M., et al., *Extracellular and Intracellular Actions of Sphingosine-1-Phosphate.* Sphingolipids as Signaling and Regulatory Molecules, 2010. **688**: p. 141-155.

27.   Nagahashi, M., et al., *Sphingosine-1-Phosphate Transporters as Targets for Cancer Therapy.* Biomed Research International, 2014.

28.   Spiegel, S. and S. Milstien, *Sphingosine 1-phosphate, a key cell signaling molecule.* Journal of Biological Chemistry, 2002. **277**(29): p. 25851-25854.

29. Hanson, M.A., et al., *Crystal Structure of a Lipid G Protein-Coupled Receptor.* Science, 2012. **335**(6070): p. 851-855.

30. Hisano, Y., T. Nishi, and A. Kawahara, *The functional roles of S1P in immunity.* Journal of Biochemistry, 2012. **152**(4): p. 305-311.

31. Lee, M.J., et al., *Sphingosine-1-phosphate as a ligand for the G protein coupled receptor EDG-1.* Science, 1998. **279**(5356): p. 1552-1555.

32. Okamoto, H., et al., *EDG1 is a functional sphingosine-1-phosphate receptor that is linked via a Gi/o to multiple signaling pathways, including phospholipase C activation, Ca2+ mobilization, Ras-mitogen-activated protein kinase activation, and adenylate cyclase inhibition.* J Biol Chem, 1998. **273**(42): p. 27104-10.

33. Yue, J., et al., *CD38/cADPR/Ca2+ pathway promotes cell proliferation and delays nerve growth factor-induced differentiation in PC12 cells.* J Biol Chem, 2009. **284**(43): p. 29335-42.

34. Ishii, I., et al., *Lysophospholipid receptors: signaling and biology.* Annu Rev Biochem, 2004. **73**: p. 321-54.

35. Okamoto, H., et al., *EDG3 is a functional receptor specific for sphingosine 1-phosphate and sphingosylphosphorylcholine with signaling characteristics distinct from EDG1 and AGR16.* Biochemical and Biophysical Research Communications, 1999. **260**(1): p. 203-208.

36. Schulze, T., et al., *Sphingosine-1-phospate receptor 4 (S1P(4)) deficiency profoundly affects dendritic cell function and TH17-cell differentiation in a murine model.* FASEB J, 2011. **25**(11): p. 4024-36.

37.   Dev, K.K., et al., *Brain sphingosine-1-phosphate receptors: Implication for FTY720 in the treatment of multiple sclerosis.* Pharmacology & Therapeutics, 2008. **117**(1): p. 77-93.

38.   Novgorodov, A.S., et al., *Activation of sphingosine-1-phosphate receptor S1P5 inhibits oligodendrocyte progenitor migration.* FASEB J, 2007. **21**(7): p. 1503-14.

39.   Awad, A.S., et al., *Chronic sphingosine 1-phosphate 1 receptor activation attenuates early-stage diabetic nephropathy independent of lymphocytes.* Kidney Int, 2011. **79**(10): p. 1090-8.

40.   Geoffroy, K., et al., *Glomerular proliferation during early stages of diabetic nephropathy is associated with local increase of sphingosine-1-phosphate levels.* FEBS Lett, 2005. **579**(5): p. 1249-54.

41.   Lai, L.W., et al., *A sphingosine-1-phosphate type 1 receptor agonist inhibits the early T-cell transient following renal ischemia-reperfusion injury.* Kidney Int, 2007. **71**(12): p. 1223-31.

42.   Park, S.W., et al., *Sphingosine kinase 1 protects against renal ischemia-reperfusion injury in mice by sphingosine-1-phosphate1 receptor activation.* Kidney Int, 2011. **80**(12): p. 1315-27.

43.   Park, S.W., et al., *Inhibition of sphingosine 1-phosphate receptor 2 protects against renal ischemia-reperfusion injury.* J Am Soc Nephrol, 2012. **23**(2): p. 266-80.

44.   Volzke, A., et al., *Sphingosine 1-phosphate (S1P) induces COX-2 expression and PGE2 formation via S1P receptor 2 in renal mesangial cells.* Biochim Biophys Acta, 2014. **1841**(1): p. 11-21.

45. Abboud, H.E., *Platelet-derived growth factor and mesangial cells.* Kidney Int, 1992. **41**(3): p. 581-3.

46. Jo, S.K., et al., *Sphingosine-1-phosphate receptors: biology and therapeutic potential in kidney disease.* Kidney Int, 2008. **73**(11): p. 1220-30.

47. Koch, A., J. Pfeilschifter, and A. Huwiler, *Sphingosine 1-Phosphate in Renal Diseases.* Cellular Physiology and Biochemistry, 2013. **31**(6): p. 745-760.

48. Nogueira, A., M. JoÃO Pires, and P. Alexandra Oliveira, *Pathophysiological Mechanisms of Renal Fibrosis: A Review of Animal Models and Therapeutic Strategies.* In Vivo, 2017. **31**(1): p. 1-22.

49. Xue, M. and C.J. Jackson, *Extracellular Matrix Reorganization During Wound Healing and Its Impact on Abnormal Scarring.* Adv Wound Care (New Rochelle), 2015. **4**(3): p. 119-136.

50. Gabbiani, G., *The myofibroblast in wound healing and fibrocontractive diseases.* Journal of Pathology, 2003. **200**(4): p. 500-503.

51. Liu, Y., *Cellular and molecular mechanisms of renal fibrosis.* Nat Rev Nephrol, 2011. **7**(12): p. 684-96.

52. Imig, J.D. and M.J. Ryan, *Immune and inflammatory role in renal disease.* Compr Physiol, 2013. **3**(2): p. 957-76.

53. Rabb, H., *The T cell as a bridge between innate and adaptive immune systems: Implications for the kidney.* Kidney International, 2002. **61**(6): p. 1935-1946.

54. Chevalier, R.L., M.S. Forbes, and B.A. Thornhill, *Ureteral obstruction as a model of renal interstitial fibrosis and obstructive nephropathy.* Kidney Int, 2009. **75**(11): p. 1145-52.

55.   Liu, Y.H., *Renal fibrosis: New insights into the pathogenesis and therapeutics.* Kidney International, 2006. **69**(2): p. 213-217.

56.   Hodgkins, K.S. and H.W. Schnaper, *Tubulointerstitial injury and the progression of chronic kidney disease.* Pediatric Nephrology, 2012. **27**(6): p. 901-9.

57.   Pan, S.Y., Y.T. Chang, and S.L. Lin, *The role of hypoxia-inducible factors in renal fibrosis.* J Formos Med Assoc, 2013. **112**(10): p. 587-8.

58.   Sun, Y.B.Y., et al., *The origin of renal fibroblasts/myofibroblasts and the signals that trigger fibrosis.* Differentiation, 2016. **92**(3): p. 102-107.

59.   Thiery, J.P., et al., *Epithelial-Mesenchymal Transitions in Development and Disease.* Cell, 2009. **139**(5): p. 871-890.

60.   Wang, W.S., V. Koka, and H.Y. Lan, *Transforming growth factor-beta and Smad signalling in kidney diseases.* Nephrology, 2005. **10**(1): p. 48-56.

61.   Li, G.B., et al., *Enhanced Epithelial-to-Mesenchymal Transition Associated with Lysosome Dysfunction in Podocytes: Role of p62/Sequestosome 1 as a Signaling Hub.* Cellular Physiology and Biochemistry, 2015. **35**(5): p. 1773-1786.

62.   Lee, U.E. and S.L. Friedman, *Mechanisms of hepatic fibrogenesis.* Best Pract Res Clin Gastroenterol, 2011. **25**(2): p. 195-206.

63.   Coresh, J., et al., *Prevalence of chronic kidney disease in the United States.* JAMA, 2007. **298**(17): p. 2038-47.

64.   Sarafidis, P.A., et al., *Hypertension awareness, treatment, and control in chronic kidney disease.* Am J Med, 2008. **121**(4): p. 332-40.

65.   Levey, A.S. and J. Coresh, *Chronic kidney disease.* Lancet, 2012. **379**(9811): p. 165-80.

66. Murphy, D., et al., *Trends in Prevalence of Chronic Kidney Disease in the United States.* Ann Intern Med, 2016. **165**(7): p. 473-481.

67. Wahba, I.M. and R.H. Mak, *Obesity and obesity-initiated metabolic syndrome: mechanistic links to chronic kidney disease.* Clin J Am Soc Nephrol, 2007. **2**(3): p. 550-62.

68. Nogueira, A., M.J. Pires, and P.A. Oliveira, *Pathophysiological Mechanisms of Renal Fibrosis: A Review of Animal Models and Therapeutic Strategies.* In Vivo, 2017. **31**(1): p. 1-22.

69. Means, C.K. and J.H. Brown, *Sphingosine-1-phosphate receptor signalling in the heart.* Cardiovascular Research, 2009. **82**(2): p. 193-200.

70. Li, C.Y., et al., *Homing of bone marrow mesenchymal stem cells mediated by sphingosine 1-phosphate contributes to liver fibrosis (vol 50, pg 1174, 2009).* Journal of Hepatology, 2009. **51**(5): p. 973-973.

71. Kono, Y., et al., *Sphingosine kinase 1 regulates differentiation of human and mouse lung fibroblasts mediated by TGF-beta 1.* American Journal of Respiratory Cell and Molecular Biology, 2007. **37**(4): p. 395-404.

72. Katsuma, S., et al., *Transcriptional profiling of gene expression patterns during sphingosine 1-phosphate-induced mesangial cell proliferation.* Biochem Biophys Res Commun, 2003. **300**(2): p. 577-584.

73. Bonner, J.C., *Regulation of PDGF and its receptors in fibrotic diseases.* Cytokine Growth Factor Rev, 2004. **15**(4): p. 255-73.

74. Schwalm, S., J. Pfeilschifter, and A. Huwiler, *Sphingosine-1-phosphate: A Janus-faced mediator of fibrotic diseases.* Biochimica Et Biophysica Acta-Molecular and Cell Biology of Lipids, 2013. **1831**(1): p. 239-250.

75. Schwalm, S., J. Pfeilschifter, and A. Huwiler, *Targeting the Sphingosine Kinase/Sphingosine 1-Phosphate Pathway to Treat Chronic Inflammatory Kidney Diseases.* Basic Clin Pharmacol Toxicol, 2014. **114**(1): p. 44-49.

76. Chevalier, R.L., M.S. Forbes, and B.A. Thornhill, *Ureteral obstruction as a model of renal interstitial fibrosis and obstructive nephropathy.* Kidney Int, 2009. **75**(11): p. 1145-1152.

77. Chaabane, W., et al., *Autophagy, apoptosis, mitoptosis and necrosis: interdependence between those pathways and effects on cancer.* Arch Immunol Ther Exp (Warsz), 2013. **61**(1): p. 43-58.

78. Wang, Z.Q., R.A. Felder, and R.M. Carey, *Selective inhibition of the renal dopamine subtype D-1A receptor induces antinatriuresis in conscious rats.* Hypertension, 1999. **33**(1): p. 504-510.

79. Junqueira, L.C., G. Bignolas, and R.R. Brentani, *Picrosirius staining plus polarization microscopy, a specific method for collagen detection in tissue sections.* Histochem J, 1979. **11**(4): p. 447-55.

80. Wang, Z., et al., *Silencing of hypoxia-inducible factor-1alpha gene attenuates chronic ischemic renal injury in two-kidney, one-clip rats.* Am J Physiol Renal Physiol, 2014. **306**(10): p. F1236-42.

81. Thallas-Bonke, V., et al., *Nox-4 deletion reduces oxidative stress and injury by PKC-alpha-associated mechanisms in diabetic nephropathy.* Physiol Rep, 2014. **2**(11).

82. Komada, T., et al., *Role of NLRP3 Inflammasomes for Rhabdomyolysis-induced Acute Kidney Injury.* Sci Rep, 2015. **5**: p. 10901.

83. Junqueira, L.C.U., G. Bignolas, and R.R. Brentani, *Picrosirius Staining Plus Polarization Microscopy, a Specific Method for Collagen Detection in Tissue-Sections.* Histochemical Journal, 1979. **11**(4): p. 447-455.

84. Cho, M.H., et al., *Orchiectomy attenuates kidney fibrosis after ureteral obstruction by reduction of oxidative stress in mice.* Am J Nephrol, 2012. **35**(1): p. 7-16.

85. Cho, M.-H., et al., *$17{beta}$-estradiol Attenuates Renal Fibrosis in Mice with Obstructive Uropathy.* Child Kidney Dis, 2011. **15**(2): p. 125-137.

86. Takuwa, N., et al., *S1P3-mediated cardiac fibrosis in sphingosine kinase 1 transgenic mice involves reactive oxygen species.* Cardiovascular Research, 2010. **85**(3): p. 484-93.

87. Li, C., et al., *Involvement of sphingosine 1-phosphate (SIP)/S1P3 signaling in cholestasis-induced liver fibrosis.* Am J Pathol, 2009. **175**(4): p. 1464-72.

88. Shiohira, S., et al., *Sphingosine-1-phosphate acts as a key molecule in the direct mediation of renal fibrosis.* Physiol Rep, 2013. **1**(7): p. e00172.

89. Han, W.Q., et al., *Hypoxia-inducible factor prolyl-hydroxylase-2 mediates transforming growth factor beta 1-induced epithelial-mesenchymal transition in renal tubular cells.* Biochimica Et Biophysica Acta-Molecular Cell Research, 2013. **1833**(6): p. 1454-1462.

90.   Xiu, L., et al., *Intracellular sphingosine 1-phosphate contributes to collagen expression of hepatic myofibroblasts in human liver fibrosis independent of its receptors.* Am J Pathol, 2015. **185**(2): p. 387-98.

91.   Ucero, A.C., et al., *Unilateral ureteral obstruction: beyond obstruction.* Int Urol Nephrol, 2014. **46**(4): p. 765-76.

92.   Higgins, D.F., et al., *Hypoxia promotes fibrogenesis in vivo via HIF-1 stimulation of epithelial-to-mesenchymal transition.* Journal of Clinical Investigation, 2007. **117**(12): p. 3810-3820.

93.   Eckardt, K.U., et al., *Role of hypoxia in the pathogenesis of renal disease.* Kidney Int Suppl, 2005(99): p. S46-51.

94.   Schreiner, G.F., et al., *Immunological aspects of acute ureteral obstruction: immune cell infiltrate in the kidney.* Kidney Int, 1988. **34**(4): p. 487-93.

95.   Misseri, R., et al., *Unilateral ureteral obstruction induces renal tubular cell production of tumor necrosis factor-alpha independent of inflammatory cell infiltration.* J Urol, 2004. **172**(4 Pt 2): p. 1595-9; discussion 1599.

96.   Meldrum, K.K., et al., *TNF-alpha neutralization decreases nuclear factor-kappaB activation and apoptosis during renal obstruction.* J Surg Res, 2006. **131**(2): p. 182-8.

97.   Morrissey, J.J. and S. Klahr, *Rapid communication. Enalapril decreases nuclear factor kappa B activation in the kidney with ureteral obstruction.* Kidney Int, 1997. **52**(4): p. 926-33.

98.   Morrissey, J.J. and S. Klahr, *Effect of AT2 receptor blockade on the pathogenesis of renal fibrosis.* Am J Physiol, 1999. **276**(1 Pt 2): p. F39-45.

99.   Sanz, A.B., et al., *NF-kappaB in renal inflammation.* J Am Soc Nephrol, 2010. **21**(8): p. 1254-62.

100.   Sakai, T., T. Kawamura, and T. Shirasawa, *Mizoribine improves renal tubulointerstitial fibrosis in unilateral ureteral obstruction (UUO)-treated rat by inhibiting the infiltration of macrophages and the expression of alpha-smooth muscle actin.* J Urol, 1997. **158**(6): p. 2316-22.

101.   Liang, J., et al., *Sphingosine-1-phosphate links persistent STAT3 activation, chronic intestinal inflammation, and development of colitis-associated cancer.* Cancer Cell, 2013. **23**(1): p. 107-20.

102.   Yu, H., M. Kortylewski, and D. Pardoll, *Crosstalk between cancer and immune cells: role of STAT3 in the tumour microenvironment.* Nature Reviews Immunology, 2007. **7**(1): p. 41-51.

103.   Ding, B.B., et al., *Constitutively activated STAT3 promotes cell proliferation and survival in the activated B-cell subtype of diffuse large B-cell lymphomas.* Blood, 2008. **111**(3): p. 1515-1523.

104.   Yu, H., D. Pardoll, and R. Jove, *STATs in cancer inflammation and immunity: a leading role for STAT3.* Nature Reviews Cancer, 2009. **9**(11): p. 798-809.

105.   Chi, H., *Sphingosine-1-phosphate and immune regulation: trafficking and beyond.* Trends Pharmacol Sci, 2011. **32**(1): p. 16-24.

106.   Anders, H.J. and M. Ryu, *Renal microenvironments and macrophage phenotypes determine progression or resolution of renal inflammation and fibrosis.* Kidney Int, 2011. **80**(9): p. 915-25.

107.   Yoo, K.H., et al., *Osteopontin regulates renal apoptosis and interstitial fibrosis in neonatal chronic unilateral ureteral obstruction.* Kidney Int, 2006. **70**(10): p. 1735-41.

108.   Chevalier, R.L., B.A. Thornhill, and A.Y. Chang, *Unilateral ureteral obstruction in neonatal rats leads to renal insufficiency in adulthood.* Kidney Int, 2000. **58**(5): p. 1987-95.

VITA

1. ## PERSONAL INFORMATION:

   1.1 Name: Xiwen Zhang

   1.2 Home Address:

   1207E, 300 West Franklin Street

   Richmond, VA 23220

   Phone: (267) 4555245

   1.3 Education Experience:

   09/2011-07/2015 Bachelor of Science, Major: <u>Pharmaceutics</u> Shenyang

   Pharmaceutical University, China

   08/2015-Present Master of Science, Major: <u>Pharmacology and</u>

   <u>Toxicology</u> Virginia Commonwealth University, USA

2. ## BIBLIOGRAPHY:

1. **Xiwen Zhang**, Fan Wang, Weili Wang, Pin-lan Li, Tien Comlekoglu, Ningjun Li, Knockout of sphingosine kinase 1 attenuates renal interstitial fibrosis in unilateral ureteral obstruction (UUO) model. FASEB J 31: 2017

2. Hongyan Wei, Juan Song, Hao Li, Yang Li, Shanshan Zhu, Xiaodan Zhou, **Xiwen Zhang**, Li Yang, Active loading liposomal irinotecan hydrochloride: Preparation, in vitro and in vivo evaluation, Asian Journal of Pharmaceutical Sciences 8(5): 303-311, 2013.

3. Xiaodan Zhou, Xiaojiao Tang, Yang Li, Zhuan Song, Haiyang Wu, **Xiwen Zhang**, Xiaorong Wang, Li Yang, Studies on oxaliplatin liposome, Conference Meeting Presentation, 2013

4. Juan Song, Hongyan Wei, Yang Li, Shanshan Zhu, Xiaodan Zhou, Xiaorong Wang, **Xiwen Zhang**, Li Yang, Influence of transmembrane ammonium salts gradient on the loading efficiency and pharmacokinetics of liposomal irinotecan hydrochloride, Conference Meeting Presentation, 2013